LPT Orsay 08-82
January 7, 2009

Phenomenology of the constrained NMSSM

A. Djouadi, U. Ellwanger and A.M. Teixeira*

Laboratoire de Physique Théorique, CNRS – UMR 8627,
Université de Paris XI, F-91405 Orsay Cedex, France

Abstract

We discuss several phenomenological aspects of the fully constrained version of the next-to-minimal supersymmetric extension of the standard model (cNMSSM). Assuming universal boundary conditions at a high energy scale for the soft supersymmetry-breaking gaugino, sfermion and Higgs masses as well as for the trilinear interactions, we find that the model can satisfy all present constraints from colliders and cosmological data on dark matter, B- and muon-physics. The phenomenologically viable region of the parameter space of the cNMSSM can be described by essentially one single parameter as the universal gaugino mass parameter $M_{1/2}$, and corresponds to small values for the universal scalar mass m_0. The lightest supersymmetric particle is always a singlino-like neutralino that is almost degenerate with the lightest tau slepton. We study the particle spectrum of the model and its signatures at the LHC, such as possibly long-lived tau sleptons at the end of decay chains, that would distinguish the cNMSSM from the constrained MSSM.

* Address after 01/11/2008: CFTP, Instituto Superior Técnico, Av. Rovisco Pais 1, 1049-001 Lisboa, Portugal.

1 Introduction

The next-to-minimal supersymmetric standard model (NMSSM) [1–3], in which the spectrum of the minimal extension (MSSM) is extended by one singlet superfield, was among the first supersymmetric (SUSY) models based on supergravity-induced SUSY-breaking terms. It has gained a renewed interest in the last decade, since it solves in a natural and elegant way the so-called μ problem [4] of the MSSM: in the NMSSM, this parameter is linked to the vacuum expectation value (vev) of the singlet Higgs field, and a value close to the SUSY-breaking scale is dynamically generated. In fact, the NMSSM is the simplest supersymmetric generalization of the standard model (SM) in which the SUSY breaking scale is the *only* scale in the Lagrangian, since it allows for a scale invariant superpotential.

In contrast to the non or partially constrained versions of the NMSSM that have been intensively studied in recent years [5] and which involve many free parameters, the constrained model (cNMSSM) has soft SUSY-breaking parameters that are universal at a high scale such as the grand unification (GUT) scale: common gaugino ($M_{1/2}$) and scalar (m_0) masses as well as trilinear couplings (A_0), as motivated by schemes for SUSY-breaking that are mediated by flavour blind gravitational interactions. If one assumes that the soft SUSY-breaking parameters involving the additional singlet sector are universal as well, the model has the same number of unknown parameters as the constrained MSSM (cMSSM) [6].

General features of the constrained NMSSM parameter space as well as aspects of its phenomenology have been discussed earlier in Refs. [2, 3]. These studies already revealed that the allowed range for the parameters $M_{1/2}$, m_0 and A_0 is different from that of the cMSSM. Small values for m_0 are disfavored in the cMSSM, as they lead to charged sleptons that are lighter than the neutralino χ_1^0, the preferred lightest SUSY particle (LSP). In the cNMSSM, small m_0 is needed to generate a non-vanishing vev of the singlet Higgs field [2]. The slepton LSP problem can be evaded owing to the presence of the additional singlino-like neutralino which, in large regions of the cNMSSM parameter space, is the true LSP [7].

Since the early studies of the cNMSSM, bounds on the Higgs and SUSY particle spectrum from high-energy collider data and low-energy measurements have become more severe, and the dark matter relic density has been determined quite accurately [8]. In addition, tools for a more precise determination of the mass spectrum and couplings [9], and for the computation of the dark matter relic density [10], have become available. In fact, the tools which allow to calculate the spectrum in the fully constrained NMSSM have only been developed recently and a brief account of the resulting phenomenology has been reported in Ref. [11]. In this paper, we investigate in more detail the parameter space of the cNMSSM in light of the recent constraints, using the updated tools.

A priori, it is not obvious if the latest constraints on the Higgs sector from LEP [12] and on the dark matter relic density [8] can be simultaneously satisfied in the fully constrained cNMSSM with its additional CP-even and CP-odd Higgs states and a singlino-like LSP. By scanning the cNMSSM parameter space with with the program NMSSMTools [9], which calculates the Higgs and SUSY particle spectra in the NMSSM, we found regions where this

is indeed possible [11]. These phenomenologically viable regions correspond to a regime of very small or vanishing universal scalar mass m_0, and the requirement of a correct relic density determines the universal trilinear A_0 as a function of the universal gaugino mass $M_{1/2}$. For low values of $M_{1/2}$, for which A_0 is also quite small, the soft SUSY-breaking terms are necessarily close to their "no-scale" values, $A_0 = m_0 = 0$ [13]. ($m_0 = 0$, but nonvanishing values for $M_{1/2}$ and A_0 at a high scale, can also originate from a strongly interacting conformal hidden sector [14]). For small enough values of the Yukawa coupling between the two doublet and the singlet Higgs fields, $\lambda \lesssim 10^{-2}$, constraints from LEP on the Higgs sector as well as constraints from B-physics are also satisfied. Notably, the model is very predictive in the sense that the complete sparticle spectrum depends essentially on just one parameter, which can be taken as $M_{1/2}$.

Moreover, in these viable regions of the parameter space, the cNMSSM can also explain the deviation of the observed anomalous magnetic moment of the muon $(g-2)_\mu$ with respect to the SM expectation [15] *as well as* the 1.7σ and $2.3\,\sigma$ excesses of events observed at LEP [12, 16] corresponding to Higgs masses around 115 GeV and 98 GeV, respectively.

Some of these results have already been published in Ref. [11]; here we discuss in more detail the full allowed parameter space, the complete sparticle and Higgs spectrum, as well as the phenomenological implications for future experiments, notably for the LHC.

An unconventional but general property of the sparticle spectrum of the cNMSSM is a singlino-like LSP with very small couplings to non-singlet particles, and a stau next-to-LSP (NLSP) with a mass close to that of the LSP. The stau will appear in practically all sparticle decay cascades. The small value of m_0 as compared to $M_{1/2}$ implies that all squarks are lighter than the gluino, a feature which will be relevant for sparticle searches at the LHC. The SM-like CP-even Higgs boson has a mass in the 115–120 GeV range.

In some regions of the parameter space of the cNMSSM, for instance for a very small Yukawa coupling λ, the stau lifetime can be very large, with visibly displaced vertices originating from its decay. For larger values of λ, the additional mostly singlet-like CP-even Higgs boson can have sizable couplings to gauge bosons and a mass around 98 GeV, which would in turn explain the $2.3\,\sigma$ excess of events observed at LEP [12, 16]; the other $1.7\,\sigma$ excess of Higgs-like events would be due to the nearly SM-like next-to-lightest CP-even Higgs with a mass close to 115 GeV.

Hence, not only the sparticle spectrum of the cNMSSM should already allow to discriminate it from the cMSSM at the LHC, but additional unconventional phenomena such as displaced vertices or a more complicated Higgs sector can also occur.

The layout of the paper is as follows: in Section 2 we describe the model, its free parameters and discuss the phenomenologically viable cNMSSM parameter space with the help of analytic approximations. In Section 3, we present the results for the Higgs and sparticle spectra. In Section 4 we discuss additional phenomenological aspects of the model that are relevant to the LHC: sparticle production cross sections and decay cascades, the possibility of displaced vertices from stau decays and features of the Higgs sector. Finally we comment on tests at e^+e^- colliders and the direct and indirect detection of dark matter, which can rule out the present model. A summary and concluding remarks are presented in Section 5.

2 The constrained NMSSM

2.1 The parameters of the cNMSSM

We consider the NMSSM with a scale invariant superpotential given by

$$\mathcal{W} = h_t\, \widehat{Q}\, \widehat{H}_u\, \widehat{t}^c_R - h_b\, \widehat{Q}\, \widehat{H}_d\, \widehat{b}^c_R - h_\tau\, \widehat{L}\, \widehat{H}_d\, \widehat{\tau}^c_R + \lambda\, \widehat{S}\, \widehat{H}_u\, \widehat{H}_d + \frac{\kappa}{3}\, \widehat{S}^3\ , \tag{2.1}$$

where hatted letters denote superfields. H_u, H_d and S represent the complex scalar Higgs fields, with h_u, h_d and s their vacuum expectation values. Tilded letters will denote the scalar components of quark and lepton superfields. For simplicity, only third generation (s)fermions have been included and $\widehat{Q}, \widehat{L}$ stand for the (t, b) and (τ, ν_τ) SU(2) doublet superfields. The three first terms in eq. (2.1) are the usual generalization of the Yukawa interactions, while the last two terms involving the singlet superfield $\widehat{S}$ substitute the $\mu \widehat{H}_u \widehat{H}_d$ term in the MSSM superpotential: a non-vanishing value s at the minimum of the Higgs potential generates an effective μ term

$$\mu_{\rm eff} \equiv \lambda\, s\ . \tag{2.2}$$

The singlet superfield $\widehat{S}$ contains a neutral CP-even and a neutral CP-odd scalar, as well as a neutralino. All these states mix with the corresponding components of the $\widehat{H}_u$ and $\widehat{H}_d$ superfields, increasing the rank of the CP-even, CP-odd and neutralino mass matrices by one as compared to the MSSM. Conventions for signs and mixing matrices are chosen as in the SLHA2 [17] convention, and we take $\lambda > 0$.

The soft SUSY–breaking terms consist of mass terms for the gaugino, Higgs and sfermion fields (for the latter, we will use the notation of the third generation; a sum over the three generations is implicitly assumed)

$$-\mathcal{L}_{\frac{1}{2}} = \frac{1}{2}\Big[M_1 \tilde{B}\tilde{B} + M_2 \sum_{a=1}^{3} \tilde{W}^a \tilde{W}_a + M_3 \sum_{a=1}^{8} \tilde{G}^a \tilde{G}_a\Big] + \text{h.c.}\ , \tag{2.3}$$

$$\begin{aligned} -\mathcal{L}_0 = {} & m^2_{H_u}|H_u|^2 + m^2_{H_d}|H_d|^2 + m^2_S|S|^2 + m^2_Q|\tilde{Q}^2| + m^2_t|\tilde{t}^2_R| \\ & + m^2_b|\tilde{b}^2_R| + m^2_L|\tilde{L}^2| + m^2_\tau|\tilde{\tau}^2_R|\ , \end{aligned} \tag{2.4}$$

as well as trilinear interactions between the sfermion and the Higgs fields, including the singlet field

$$\begin{aligned} -\mathcal{L}_{\rm tril} = {} & \Big(h_t A_t\, \tilde{Q}\, H_u\, \tilde{t}^c_R - h_b A_b\, \tilde{Q}\, H_d\, \tilde{b}^c_R - h_\tau A_\tau\, \tilde{L}\, H_d\, \tilde{\tau}^c_R \\ & + \lambda A_\lambda\, H_u\, H_d\, S + \frac{1}{3}\kappa A_\kappa\, S^3\Big) + \text{h.c.}\ . \end{aligned} \tag{2.5}$$

All parameters in the above Lagrangian depend on the energy scale via the corresponding RG equations, so that the dominant radiative corrections involving large logarithms are accounted for. In the fully constrained cNMSSM, one imposes unification of the soft SUSY–breaking gaugino masses, sfermion and Higgs masses as well as trilinear couplings at the

grand unification scale $M_{\rm GUT}$:

$$\begin{aligned} &M_1 = M_2 = M_3 \equiv M_{1/2}\,, \\ &m_{H_u} = m_{H_d} = m_S = m_Q = m_t = m_b = m_L = m_\tau \equiv m_0\,, \\ &A_t = A_b = A_\tau = A_\lambda = A_\kappa \equiv A_0\,. \end{aligned} \tag{2.6}$$

Then, apart from gauge and quark/lepton Yukawa couplings, the Lagrangian of the cNMSSM depends on the five input parameters

$$M_{1/2}\ ,\ m_0\ ,\ A_0\ ,\ \lambda \text{ and } \kappa\,. \tag{2.7}$$

Requiring the correct value of M_Z reduces the dimension of the parameter space from five to four.

In principle, one could start with four independent parameters (such as $m_0/M_{1/2}$, $A_0/M_{1/2}$, λ and κ), and integrate the RG equations for all soft terms from $M_{\rm GUT}$ down to the SUSY scale $M_{\rm SUSY}$, defined by the order of magnitude of the soft SUSY-breaking terms. Subsequently, one could minimize the effective potential with respect to h_u, h_d and s and determine the overall scale of the soft terms in eq. (2.7) from the correct value of M_Z, as done in Ref. [2]. However, since $\tan\beta = h_u/h_d$ is then obtained as output (while the top quark Yukawa coupling h_t would be an input), it becomes very difficult to obtain the correct value for the top quark mass m_t or, given m_t, h_t can only be obtained once $\tan\beta$ is known. Since h_t is very important for the radiative corrections and the RG evolution, it is much more convenient to allow for $\tan\beta$ as an input parameter, which permits to determine h_t at the weak scale from the beginning in terms of m_t.

All in all, the following procedure is feasible in practice: apart from M_Z, the five parameters

$$M_{1/2}\ ,\ m_0\ ,\ A_0\ ,\ \lambda \text{ and } \tan\beta \tag{2.8}$$

are allowed as inputs. The parameters κ, the soft singlet mass m_S^2 as well as the vev $|s|$ (or $|\mu_{\rm eff}| \equiv \lambda|s|$) are determined at $M_{\rm SUSY}$ through the three minimization equations of the scalar potential with respect to h_u, h_d and s. (With the convention $\lambda > 0$, κ typically turns out to be positive as well, and of $\mathcal{O}(\lambda/10)$; the sign of s or $\mu_{\rm eff}$ can still be chosen at will.) This is the procedure employed by the routine NMSPEC within NMSSMTools [9], which calculates the spectra of the Higgs and SUSY particles in the NMSSM in terms of the soft SUSY breaking terms at $M_{\rm GUT}$ (except for the parameter m_S^2), $\tan\beta$ at the weak scale (defined by M_Z) and λ at the SUSY scale $M_{\rm SUSY}$.

Clearly, the soft singlet mass squared m_S^2 at $M_{\rm GUT}$ will not coincide with m_0^2 in general (for a recent analysis allowing for a non-universal singlet mass term, see Ref. [18]). However, one can confine oneself to regions in parameter space where the difference between m_S^2 and m_0^2 is negligibly small. This condition leaves us with an effective 4-dimensional parameter space, consistent with the considerations above. In practice, we determine $\tan\beta$ by the requirement that m_S^2 at $M_{\rm GUT}$ should be close to m_0^2: we impose $|m_S^2(M_{\rm GUT}) - m_0^2| < (5\text{ GeV})^2$, which typically requires to tune the fourth decimal of $\tan\beta$. This should not be interpreted as a fine-tuning, since m_S^2 should be considered as an input parameter, whereas $\tan\beta$ is determined by the minimization of the effective potential.

For the most relevant SM parameters, the strong coupling and the bottom/top quark masses, we chose $\alpha_s(M_Z) = 0.1172$, $m_b^{\overline{\rm MS}}(m_b) = 4.214$ GeV and $m_t^{\rm pole} = 171.4$ GeV [19].

2.2 Constraints from the scalar potential

Let us begin by recalling some conditions on the parameters $M_{1/2}$, m_0 and A_0 of the cNMSSM, which follow from a phenomenologically acceptable minimum of the Higgs potential [2]. First, the vev s of the singlet has to be non-vanishing. The dominant s-dependent terms in the Higgs potential are given by

$$V(s) \sim \kappa^2 \, s^4 + \frac{2}{3} \kappa \, A_\kappa \, s^3 + m_S^2 \, s^2 + \dots \, , \tag{2.9}$$

and one easily finds that the condition for a non-vanishing value for s at the absolute minimum is equivalent to the inequality

$$m_S^2 \lesssim \frac{1}{9} A_\kappa^2 \, . \tag{2.10}$$

For small λ and κ (as will be the case below), the parameters A_κ and m_S are hardly renormalized between the GUT and the electroweak scales, and the above condition translates into the first constraint on the parameter space (assuming $m_0^2 \geq 0$)

$$m_0 \lesssim \frac{1}{3} |A_0| \, . \tag{2.11}$$

Next, we consider the CP-odd Higgs boson mass matrix. The dominant term in its singlet-like diagonal element is given by [1–3, 9, 17]

$$-3 \kappa A_\kappa s, \tag{2.12}$$

and must be positive. For positive s and κ this implies negative trilinear couplings

$$A_\kappa \sim A_0 < 0 \, . \tag{2.13}$$

We must also consider the constraints on the parameter space arising from vacuum stability. Dangerous instabilities of the scalar potential along charge and colour breaking (CCB) directions in field space can occur [2, 20], notably for large values of $|A_0|$. The most dangerous CCB direction is along the D-flat direction

$$|E_1| = |L_1| = |H_d| \tag{2.14}$$

in field space, where E_1 and L_1 are the right- and left-handed selectron fields, and where the term $\sim h_e A_e$ in the scalar potential can give a large negative contribution. Once A_e and the corresponding soft masses at the appropriate scale (using the corresponding RG equations) are expressed in terms of A_0, $M_{1/2}$ and m_0, the condition for the absence of such a charge and colour breaking minimum becomes [2]

$$\left(A_0 - 0.5 \, M_{1/2}\right)^2 \lesssim 9 \, m_0^2 + 2.67 \, M_{1/2}^2 \, . \tag{2.15}$$

In our analysis we will obtain relatively small values for A_0 ($A_0 \sim -\frac{1}{4} M_{1/2}$, cf. Fig. 1 below), for which eq. (2.15) is satisfied independently of the value of m_0.

More delicate could be unbounded-from-below (UFB) directions in field space, which are both D-flat and F-flat. In Ref. [20], it has been clarified that such dangerous directions in the field space of the MSSM are still present in the NMSSM, although the singlet vev s gives an additional positive contribution to the potential. Analytic approximations to the potential along such dangerous directions have been studied in Ref. [21], with the following results:

i) the inequality $m_0 \gtrsim 0.3\, M_{1/2}$ (for the large $\tan\beta$ which will be relevant here) is an approximate condition for the absence of deeper minima in these directions – this inequality will be violated below;

ii) the decay rate of the standard vacuum is usually much larger than the age of the universe; hence we have to assume that the early cosmology (temperature-induced positive masses squared for the squarks and sleptons) places us into the local standard minimum of the scalar potential.

2.3 Constraints from the dark matter relic density

In the cMSSM, small values of m_0 give rise to a stable charged slepton LSP, which would be an unacceptable dark matter candidate. The slepton LSP problem in the cMSSM with small m_0 can be evaded in the cNMSSM due to the presence of the additional singlino-like neutralino which, in large regions of the parameter space, is the true LSP [7]. However, in order to be a good dark matter candidate, its relic density should comply with the WMAP constraint [8]

$$0.094 \lesssim \Omega_{\chi_1^0} h^2 \lesssim 0.136 \qquad (\text{at } 2\,\sigma)\,. \tag{2.16}$$

In the case of a singlino-like LSP, the upper bound on the relic density implies that the singlino-like LSP mass m_{χ_S} $(= m_{\chi_1^0})$ has to be close to (but somewhat below) the mass of the NLSP, which in the present case is always the lighter (mostly right-handed) stau $\tilde{\tau}_1 \sim \tilde{\tau}_R$:

$$m^2_{\chi_S} \sim m^2_{\tilde{\tau}_R}\,. \tag{2.17}$$

Only then can the singlino co-annihilate sufficiently rapidly with the NLSP. The condition for nearly degenerate stau and singlino masses can be obtained by replacing in the singlino mass squared, $m^2_{\chi_S} \sim 4\kappa^2 s^2$ [1–3, 9, 17], the analytic approximation for the singlet vev as obtained from eq. (2.9),

$$s \approx \frac{1}{4\kappa}\left(-A_\kappa + \sqrt{A_\kappa^2 - 8 m_S^2}\right)\,. \tag{2.18}$$

Noticing again that $A_\kappa \sim A_0$ (< 0) and $m_S^2 \sim m_0^2$, $m^2_{\chi_S}$ is approximately given by

$$m^2_{\chi_S} \simeq \frac{1}{2}\left(A_0^2 + |A_0|\sqrt{A_0^2 - 8 m_0^2}\right) - 2 m_0^2\,. \tag{2.19}$$

An analytic approximation for the right-handed stau mass at the weak scale, obtained by integrating the RG equations, is given by [2]

$$m^2_{\tilde{\tau}_R} \sim m_0^2 + 0.1\, M_{1/2}^2\,. \tag{2.20}$$

Inserting eqs. (2.19) and (2.20) into eq. (2.17) and using eq. (2.11), one can derive the bound

$$m_0^2 \lesssim \frac{1}{15} M_{1/2}^2. \tag{2.21}$$

In practice, however, all approximations above (notably the neglected $\tilde{\tau}_R - \tilde{\tau}_L$ mixing) tend to overestimate m_0, and the stronger bound

$$m_0 \lesssim \frac{1}{10} M_{1/2} \tag{2.22}$$

holds. Hence, m_0 must be quite small when compared to $M_{1/2}$, and could well vanish.

These analytic approximations allow to understand which "hyperplane" in the parameter space $M_{1/2}$, m_0 and A_0 will satisfy the WMAP constraint of eq. (2.16): not only must m_0 be small, but A_0 is essentially determined in terms of $M_{1/2}$ by eq. (2.17). Our numerical results (for $m_0 \sim 0$, see below) correspond to

$$A_0 \sim -\frac{1}{4} M_{1/2} \; . \tag{2.23}$$

Finally, as in the cMSSM [22], the WMAP constraint also requires that $M_{1/2}$ should not be too large. Since the dominant annihilation process of R-odd sparticles is now $\tilde{\tau}_1 + \tilde{\tau}_1 \to$ SM particles, the rate decreases with $m_{\tilde{\tau}_1}$ (which is roughly proportional to $M_{1/2}$), eventually becoming too small for $M_{1/2} \gtrsim 2$–3 TeV.

The routine NMSSMTools [9], which includes a version of the dark matter tool MicrOMEGAS [10] adapted to the NMSSM, allows to scan the parameter space of the cNMSSM and to verify which parameters $M_{1/2}$, m_0 and A_0 satisfy the WMAP constraint, eq. (2.16). We recall that λ is another free parameter of the model, whereas $\tan\beta$ is fixed by the condition $m_S = m_0$ at the GUT scale. In the next subsection we will discuss that LEP constraints impose an upper bound on λ, $\lambda \lesssim 10^{-2}$, and, for illustrative purposes, we will fix $\lambda = 0.002$ throughout the remaining part of this subsection. In any case, the following results are practically independent of λ.

In Fig. 1 we show the allowed range of the parameters m_0 and A_0 as functions of $M_{1/2}$. In the left panel, we display the contours for the minimal and maximal values of m_0. We notice that $m_0 = 0$ is only compatible with the WMAP constraint for $M_{1/2} \lesssim 2$ TeV. Moreover, as $M_{1/2}$ increases, it becomes increasingly difficult to satisfy the WMAP constraint and, hence, the allowed range for m_0 decreases. For $M_{1/2} > 3$ TeV, hardly any parameter space survives since $\Omega_{\chi_1^0} h^2$ would be too large.

In the right panel of Fig. 1, we present the values of A_0 corresponding to the maximal and minimal values of m_0 for a given $M_{1/2}$ (we recall that eq. (2.16) fixes A_0 in terms of $M_{1/2}$ and m_0). Likewise, we display the values of $\tan\beta$ obtained from the requirement of full scalar mass unification $m_S^2 \simeq m_0^2$.

We notice that $\tan\beta$ turns out to be quite large (see Ref. [23] for earlier work on the NMSSM at large $\tan\beta$). The origin of the large value of $\tan\beta$ can be understood as follows. First, an effective B-parameter

$$B_{\rm eff} = A_\lambda + \kappa s \tag{2.24}$$

can be defined, which plays the same rôle as the B-parameter of the MSSM. Then, $\tan\beta$ is inversely proportional to $\sim |B_{\rm eff}|$. In the regime where $m_S^2 \sim m_0^2 \ll A_0^2 \sim A_\kappa^2$, eq. (2.18)

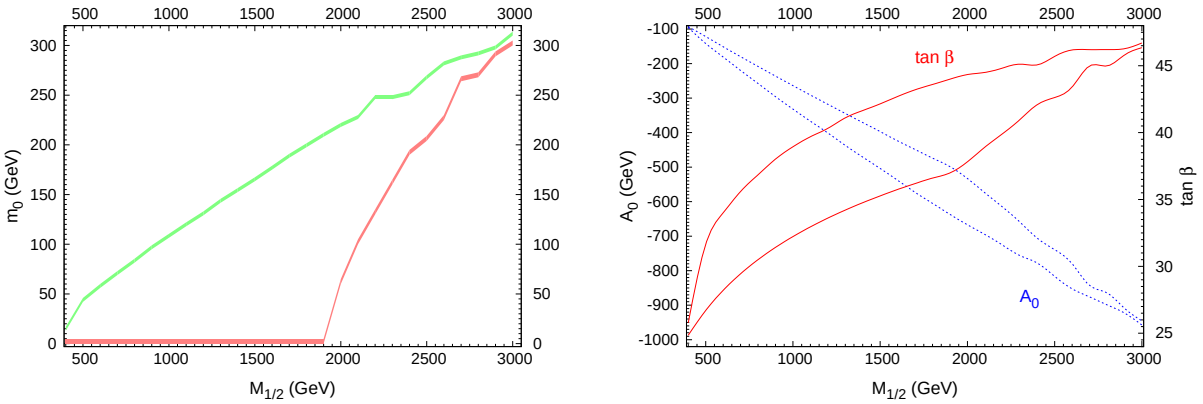

Figure 1: In the left panel, maximal and minimal values of m_0 allowed by the WMAP constraint of eq. (2.16), as a function of $M_{1/2}$ (in GeV). In the right panel, associated range of A_0 (in GeV) and $\tan\beta$, also as a function of $M_{1/2}$. In the case of $\tan\beta$ (A_0), the lower (upper) line corresponds to $m_0 = 0$.

gives $s \sim -A_\kappa/2\kappa$, and thus $B_{\rm eff} \approx A_\lambda - \frac{1}{2}A_\kappa$ with $A_\kappa \sim A_0$ and A_λ determined by the RG equations. Finally, accidentally, $A_\lambda - \frac{1}{2}A_\kappa$ happens to be small (much smaller than $\mu_{\rm eff}$) leading to $\tan\beta \gg 1$.

The lower limit on $M_{1/2}$ of ~ 400 GeV follows from the lower bound on the lightest stau mass of ~ 100 GeV from the negative LEP searches [19]. The corresponding lower limit on $M_{1/2}$ derived from eq. (2.20) seems somewhat weaker, but the stau mixing has to be taken into account. For $M_{1/2} \approx 400$ GeV, we observe from Fig. 1 that only $m_0 \lesssim 20$ GeV is viable. For larger values of $M_{1/2}$, values for m_0 up to $\sim \frac{1}{10}M_{1/2}$ are possible (with sizable values of $\tan\beta \gtrsim 40$). For values of $M_{1/2}$ larger than 2 TeV, compatibility with the correct dark matter relic density (which requires $M_{1/2} < 2$ TeV for $m_0 = 0$) can no longer be obtained for $m_0 = 0$: the increasingly larger values of $\tan\beta$, as determined by the requirement of scalar mass unification at the GUT scale, generate a stronger mixing in the stau sector. Then, in order to have $m_{\tilde\tau_1} \gtrsim m_{\chi_1^0}$, a non-vanishing, albeit small, value of m_0 is required. For $m_0 \neq 0$, compatibility with the WMAP bound allows for $M_{1/2}$ up to around 3 TeV, where $m_0 \sim 300$ GeV and $\tan\beta \sim 46$, with the upper bound on m_0 following from eq. (2.11).

Restricting ourselves to the phenomenologically more interesting regime $M_{1/2} \lesssim 1.5$ TeV, we present in Fig. 2 several WMAP-compatible "lines" in the $[M_{1/2}, A_0]$ plane for fixed values of m_0. Actually, the allowed $2\,\sigma$ range for Ωh^2 implies that the lines displayed correspond to "bands" of finite (yet small) width. The parameter space lying below these lines is typically excluded due to the presence of a stau LSP (and to a minor extent, also a violation of the WMAP constraint). The upper regions delimited by each line are excluded due to an excessively large relic density.

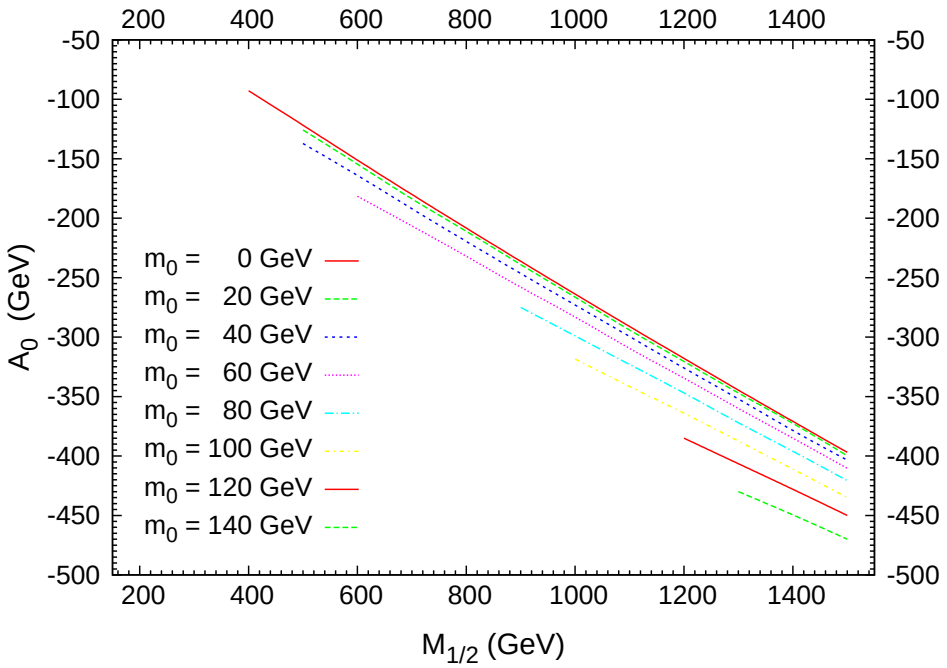

Figure 2: Distinct allowed "lines" in the $[M_{1/2}, A_0]$ plane compatible with the WMAP constraint of eq. (2.16). From top to bottom, the lines correspond to decreasing values of $m_0 = 0$ from 20 to 140 GeV.

2.4 Constraints on λ from LEP and dark matter

Remarkably, LEP constraints on the SM-like Higgs boson mass turn out to be satisfied due to the relatively large stop masses and trilinear coupling A_t for *all* parameter ranges shown in Figs. 1 and 2. However, they lead to upper bounds on the NMSSM specific parameter λ. For the large values of $\tan\beta$ obtained in this scenario, a large value of λ does *not* lead to an increase of the SM-like Higgs mass. On the contrary, increasing λ simply increases the mixing of the singlet-like CP-even scalar with doublet-like CP-even scalars. If the singlet-like CP-even scalar mass is larger, the SM-like Higgs mass decreases with increasing λ and can fall below the LEP bound. If the singlet-like CP-even scalar mass is below the SM-like Higgs mass limit, i.e. $\lesssim 114$ GeV, its coupling to the Z-boson, which is proportional to λ, must be sufficiently small, equally implying an upper bound on λ.

In Fig. 3, we show the corresponding upper limits on λ for the case $m_0 = 0$. The constraint is particularly strong in the "cross-over" region near $M_{1/2} \sim 660$ GeV (see Fig. 5 below), where relatively small values of λ can generate a large mixing angle. We see that $\lambda \lesssim 10^{-2}$ is required for all values of $M_{1/2}$; hence, the parameter λ will have practically no effect on the remaining spectrum except for the singlet-like Higgs masses.

On the other hand, a rough lower bound on λ can be derived from the efficiency of singlino-like LSP annihilation in the early universe. For the dilution of the LSP, two processes are relevant in the limit of small λ. The dominant annihilation process of R-odd

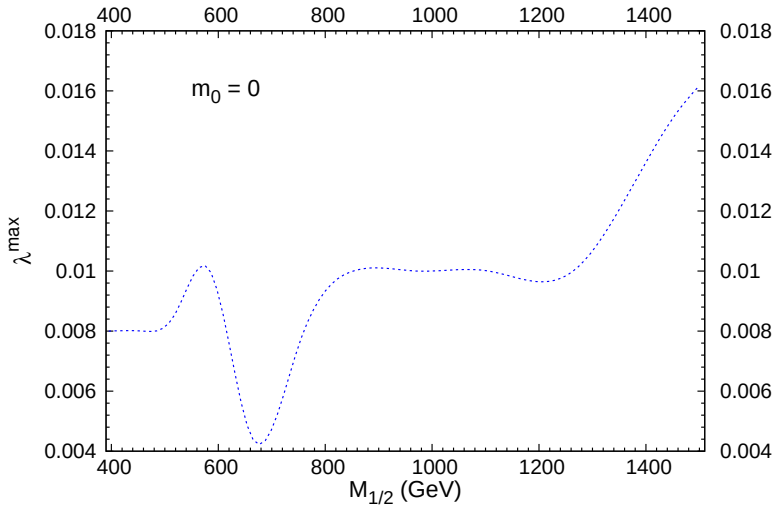

Figure 3: The upper bound on the parameter λ as a function of $M_{1/2}$ (in GeV), as obtained from LEP constraints on the NMSSM Higgs sector; for simplicity, we set $m_0 = 0$.

particles is NLSP + NLSP $\to X$, the NLSP being the lightest stau. The reaction rate for this process is given by $(n_{\rm NLSP})^2\sigma$, where $n_{\rm NLSP}$ is the corresponding time and temperature dependent abundance, and σ is the thermally averaged cross section.

The other relevant process leading to the observed relic density is LSP$+X \to$ NLSP$+X'$ (and its inverse), where X and X' are practically massless quarks and leptons – this process helps to maintain the LSP and the NLSP in thermal equilibrium. Its reaction rate can be written as $n_{\rm LSP}\, n_X\, \sigma'$, and depends on the small, but non-vanishing, non-singlet component of the singlino-like LSP of $\mathcal{O}(\lambda/g_2)$, where g_2 is the SU(2) coupling constant. Consequently, the cross section σ' is $\sim \lambda^2/g_2^2 \times \sigma$, and is correspondingly suppressed for small λ.

Nevertheless, the process LSP$+X \to$ NLSP$+X'$ is typically faster than the annihilation process NLSP + NLSP $\to X$, since near the freeze-out temperature, the abundance n_X of quarks and leptons is $\sim 10^9$ larger than the abundances of the LSP and NLSP (for $m_{\rm LSP} \sim m_{\rm NLSP}$) [24]. This allows to dilute the LSP density as fast as the NLSP density.

Only for very small λ, the reaction rate of the process LSP + $X \to$ NLSP + X' can become smaller than the one for NLSP + NLSP $\to X$; then the LSP will no longer be in thermal equilibrium with the NLSP near the freeze-out temperature, but can be considered as decoupled, implying an excessively large relic density. According to the discussion above, this would happen for $\lambda^2/g_2^2 \lesssim 10^{-9}$ or $\lambda \lesssim 10^{-5}$. Clearly, these are rough estimates, which would merit more detailed investigations. In the following, we employ values of λ sufficiently above 10^{-5} such that the hypothesis of thermal equilibrium between the LSP and the NLSP near the relevant temperature can be considered as satisfied.

We remark that, even if we hypothetically allowed for other contributions to the dark matter relic density, this would not affect the lower bound for λ estimated above, nor the previous discussion on the allowed parameter space (i.e., the derived bounds on $M_{1/2}$, m_0,

etc.), since all bounds originate from the *upper* WMAP limit on the relic density.

2.5 Constraints from flavor physics

As previously mentioned, we have checked that constraints from B-meson physics [25] are satisfied. More precisely, agreement within $2\,\sigma$ between the following observables and their theoretical values is verified by the NMSSMTools routine [9]: the decay branching ratios $\mathrm{BR}(B \to X_s\gamma)$, $\mathrm{BR}(\bar{B}^+ \to \tau^+\nu_\tau)$, $\mathrm{BR}(B_s \to \mu^+\mu^-)$ and the mass differences ΔM_q, $q = d, s$. It turns out that all regions in parameter space investigated before (i.e. consistent with WMAP and collider constraints) are also allowed by constraints from B-physics.

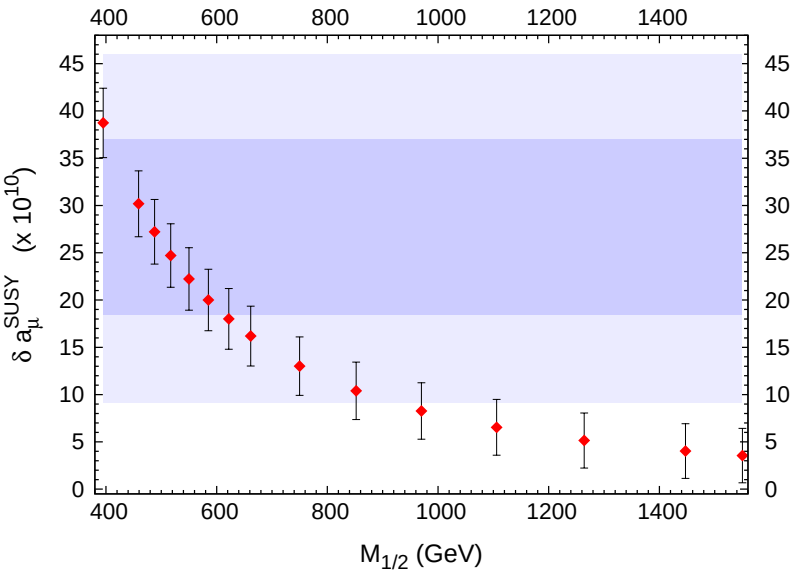

Figure 4: $\delta a_\mu^{\mathrm{SUSY}}$ as a function of $M_{1/2}$ (in GeV) for $m_0 = 0$. The vertical bars denote the theoretical error, while darker (lighter) regions correspond to a $1\,\sigma$ ($2\,\sigma$) deviation from the central value of $a_\mu^{\mathrm{exp}} - a_\mu^{\mathrm{SM}}$; data taken from Ref. [27].

More important constraints arise from requiring that SUSY accounts for the $\sim 3\,\sigma$ deviation of the observed anomalous magnetic moment of the muon with respect to the SM expectation[1], $\delta a_\mu^{\mathrm{SUSY}} = (27.7 \pm 9.3) \times 10^{-10}$ [15]. The cNMSSM has been analysed in this respect in Ref. [27], the analysis being conducted for simplicity for $m_0 = 0$, but this result is practically independent of m_0. In Fig. 4, we show $\delta a_\mu^{\mathrm{SUSY}} = (g-2)_\mu^{\mathrm{SUSY}}$ as a function of $M_{1/2}$, depicting the $1\,\sigma$ and $2\,\sigma$ bands as well.

We see that the constraint from a_μ would confine the allowed range of $M_{1/2}$ to $M_{1/2} \lesssim 1$ TeV at the $2\,\sigma$ level, and to 400 GeV $\lesssim M_{1/2} \lesssim$ 600 - 700 GeV (where the sparticle spectrum is not too heavy) at the $1\,\sigma$ level. In fact, the present experimental value could be matched to arbitrarily high precision, and a more precise measurement of a_μ would eventually lead to a prediction of $M_{1/2}$ in the cNMSSM. In any case, in view of the desired value for $\delta a_\mu^{\mathrm{SUSY}}$, the region $M_{1/2} \lesssim 1$ TeV is preferred.

[1] A recent measurement of the hadronic cross section $e^+e^- \to$ hadrons using radiative return by the BaBar collaboration indicates that this discrepancy might be smaller than presently thought [26].

3 Higgs and sparticle spectra

We now proceed to analyse in some detail the Higgs and sparticle spectra obtained in the allowed regions of the cNMSSM parameter space, after imposing the bounds from Higgs and sparticle searches at LEP, the B-meson constraints and the requirement of a correct cosmological relic density as measured by WMAP for the neutralino LSP.

3.1 The Higgs spectrum

The Higgs sector of the (c)NMSSM contains three neutral CP-even Higgs states h_i^0 ($i = 1,\ 2,\ 3$), two neutral CP-odd Higgs states a_i^0 ($i = 1,\ 2$), and the charged Higgs states $h^\pm$. Their masses depend essentially on the gaugino mass parameter $M_{1/2}$.

As in the MSSM in the decoupling regime (see Ref. [28] for a review), the heaviest CP-even, CP-odd and charged Higgs states form a practically degenerate SU(2) multiplet with a common mass above 500 GeV. The mostly SM-like CP-even state has a mass increasing slightly with $M_{1/2}$ from 115 GeV up to ~ 120 GeV. This mass range is only slightly above the lower limit of 114.4 GeV on the SM Higgs boson mass, and is compatible with the Higgs mass range favored by electroweak precision data as recently obtained from a global fit (in which the central mass value is 116 GeV) [29].

The third CP-even state has a dominant singlet component; it is the only Higgs state whose mass depends – apart from $M_{1/2}$ – on m_0 and, to some extent, on λ: for small $M_{1/2}$ it is lighter than the SM-like Higgs boson, escaping LEP constraints due to the very small coupling to the Z boson. For increasing values of $M_{1/2}$, its mass increases until it becomes nearly degenerate with the SM-like CP-even Higgs state: in this region of parameter space, which will be subsequently denoted as the "cross-over" region, the singlet-like and SM-like Higgs states strongly mix. For still larger values of $M_{1/2}$, the mass of the singlet-like state exceeds the one of the SM-like state.

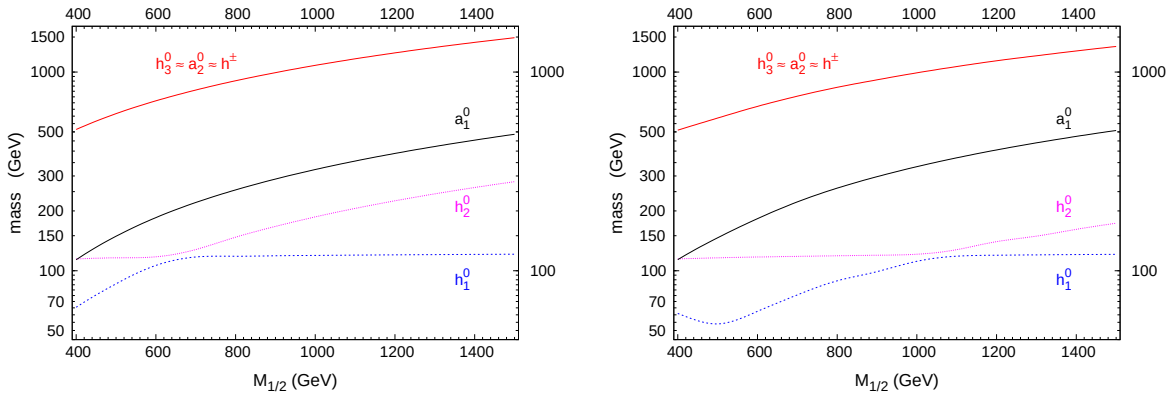

Figure 5: The Higgs masses as a function of $M_{1/2}$ (in GeV). In the left panel we set $m_0 = 0$, while in the right panel m_0 is given by its maximal value, $m_0^{\rm max}(M_{1/2})$. From below, the displayed lines correspond to the states h_1^0 (blue/dotted), h_2^0 (pink/dashed), a_1^0 (full/black) and a_2^0 (full/red) which is degenerate with the h_3^0 and $h^\pm$ states.

This "cross-over" phenomenon is visible in Fig. 5, where we display the masses of the neutral CP-even, CP-odd, and charged Higgs bosons as a function of the parameter $M_{1/2}$. On the left-hand side, we take $m_0 = 0$, while on the right-hand side we assume $m_0 = m_0^{\max}(M_{1/2})$, as given by the upper line in the left panel of Fig. 1. (With the exception of the CP-odd a_1^0 state, the Higgs mass spectrum is somewhat heavier in the case $m_0 = 0$.)

In Fig. 5 we have set $\lambda = 0.002$; then, for $m_0 = 0$ corresponding to the left panel, the "cross-over" phenomenon occurs at $M_{1/2} \sim 660$ GeV: for $M_{1/2} \lesssim 660$ GeV, the lightest CP-even state h_1^0 is singlet-like, whereas the lightest CP-even state h_1^0 is SM-like for $M_{1/2} \gtrsim 660$ GeV. In the case $m_0 = m_0^{\max}(M_{1/2})$ displayed in the right panel of Fig. 5, the corresponding "cross-over" occurs at $M_{1/2} \sim 1100$ GeV. Intermediate regimes for m_0 (with $m_0 \neq 0$) will imply a "cross-over" that takes place for $660 \lesssim M_{1/2} \lesssim 1100$ GeV.

For the present value of $\lambda = 0.002$, the CP-even singlet mass can be as small as 60 GeV for $m_0 = m_0^{\max}(M_{1/2})$ (in the right panel). For larger values of λ, close to the upper bound shown in Fig. 3, even lower $m_{h_1^0}$ values can be obtained, as will be discussed later.

The lighter singlet-like CP-odd scalar a_1^0 has a mass above ~ 120 GeV (increasing with $M_{1/2}$); the heaviest CP-even and CP-odd scalars h_3^0 and a_2^0 are practically degenerate in mass with the charged Higgs boson $h^\pm$, with masses above ~ 520 GeV.

3.2 A possible explanation of the excess in Higgs searches at LEP

In addition to the $1.7\,\sigma$ signal for a SM–like CP-even Higgs particle with a mass close to 115 GeV, the combined results on Higgs searches of the four LEP experiments via the Higgs-strahlung process $e^+e^- \to h\,Z$, followed by the Higgs decay $h \to b\bar{b}$, show a $2.3\,\sigma$ excess of events corresponding to a Higgs mass around 98 GeV [12, 16]. The number of excess events amounts to about 10% of those expected for a SM Higgs boson $h^{\rm SM}$ with the same mass. It can be explained either

i) by a reduced coupling of a candidate Higgs boson to the SM gauge bosons, $C_h^V = g_{hZZ}/g_{h^{\rm SM}ZZ} \approx \mathcal{O}(\sqrt{0.1})$,

ii) by a reduced branching ratio of a candidate Higgs boson into $b\bar{b}$ final states.

In the unconstrained MSSM, the two excesses can be explained [30] by the presence of a SM-like Higgs boson with a mass of ≈ 115 GeV (the heavier CP-even H state), while the lighter CP-even state h has a mass close to ≈ 98 GeV and reduced couplings to the Z boson.

Within the context of the unconstrained NMSSM, the explanation *ii*) of the excess for Higgs masses around 98 GeV has been proposed [31]. In this case, one can have a CP-even Higgs boson with a corresponding mass and SM-like ZZh couplings, i.e. $C_h^V \sim \mathcal{O}(1)$, but a reduced branching ratio into $b\bar{b}$ final states due to a dominant decay into pairs of very light CP-odd bosons $h_1^0 \to a_1^0\,a_1^0$ with $m_{a_1^0} < 2m_b$. Then, the light pseudoscalar a_1^0 can only decay into $\tau^+\tau^-$ and eventually light quark and gluon pairs, rendering it compatible with corresponding searches at LEP [12].

In the cNMSSM, the parameter space somewhat below the cross-over regions contains neutral Higgs scalars with masses ~ 100 GeV and couplings $C_{h_1^0}^V \approx \mathcal{O}(\sqrt{0.1})$. As an example, for 560 GeV $\lesssim M_{1/2} \lesssim 575$ GeV (with $m_0 = 0$ and $\lambda = 0.005$), one finds for the masses of

the two lighter CP-even Higgs states 97 GeV $\lesssim m_{h_1^0} \lesssim$ 101 GeV and $m_{h_2^0} \approx 117$ GeV. In this case, the reduced coupling of the lightest scalar Higgs boson to SM gauge bosons would lie in the range $0.28 \lesssim |C^V_{h_1^0}| \lesssim 0.33$ for h_1^0, so that the cNMSSM could indeed account for the observed $2.3\,\sigma$ excess around $m_h \approx 98$ GeV at LEP. In addition, since the mass of the nearly SM–like h_2^0 state is $m_{h_2^0} \approx 117$ GeV with $|C^V_{h_2^0} \sim 0.9|$, and in view of the error of a few GeV in the determination of the radiative corrections to the Higgs masses (expected to be, as in the MSSM, of the order of 3 GeV, see e.g. Ref. [32]), the $1.7\,\sigma$ excess at a Higgs mass ≈ 115 GeV could be explained as well.

Thus, in the cNMSSM, the region in parameter space corresponding to small $M_{1/2}$ can describe not only the deviation of the $(g-2)_\mu$ from the SM expectation, but both excesses of Higgs–like events at LEP as well.

3.3 The sparticle spectrum

Let us now turn to the sparticle spectrum, starting with the neutralino and slepton mass spectra shown in Fig. 6. As for the Higgs bosons, we display the case $m_0 = 0$ in the left-hand panel, and $m_0 = m_0^{\rm max}(M_{1/2})$ in the right-hand panel.

The two nearly degenerate sets of lower lines in both panels correspond to the masses of the χ_1^0 singlino-like LSP (blue/dotted) and the lighter stau $\widetilde{\tau}_1$ NLSP (red/full). The mass difference between these two states is smaller than ~ 8 GeV, as required in order to obtain a cosmological relic density for the singlino χ_1^0 compatible with WMAP.

The pattern for the masses of the charginos and the heavier neutralinos (blue/dotted lines) follows the one of the MSSM, once the proper relabeling of the states is made. Since the low-energy value of the higgsino mass parameter $\mu_{\rm eff}$ is generally quite large, $\mu_{\rm eff} \gtrsim M_2$, the heavier neutralino states χ_4^0 and χ_5^0 are higgsino-like with masses $\sim \mu_{\rm eff}$. The states χ_2^0 and χ_3^0 are, respectively, bino and wino-like with masses $m_{\chi_3^0} \approx 2 m_{\chi_2^0} \approx M_2$

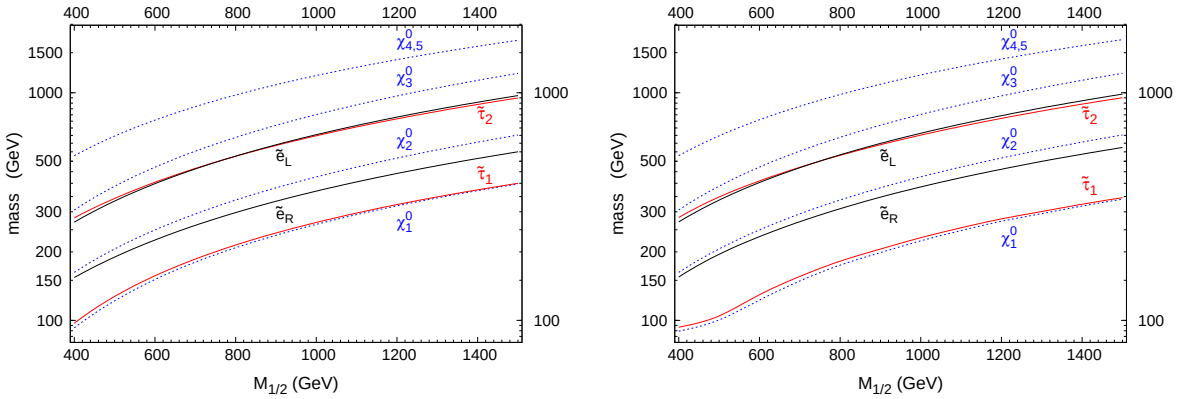

Figure 6: Neutralino (blue/dotted lines), selectron (black/full lines) and stau (red/full lines) masses as a function of $M_{1/2}$ (in GeV); on the left-hand side we set $m_0 = 0$, while on the right-hand side we set $m_0 = m_0^{\rm max}(M_{1/2})$. In both panels the states are ordered in mass as $m_{\chi_1^0} \lesssim m_{\tilde{\tau}_1} < m_{\tilde{e}_R} < m_{\chi_2^0} < m_{\tilde{\tau}_2} \lesssim m_{\tilde{e}_L} < m_{\chi_3^0} < m_{\chi_{4,5}^0}$. The charginos $\chi_1^\pm$ and $\chi_2^\pm$ are degenerate in mass with, respectively, χ_3^0 and $\chi_{4,5}^0$.

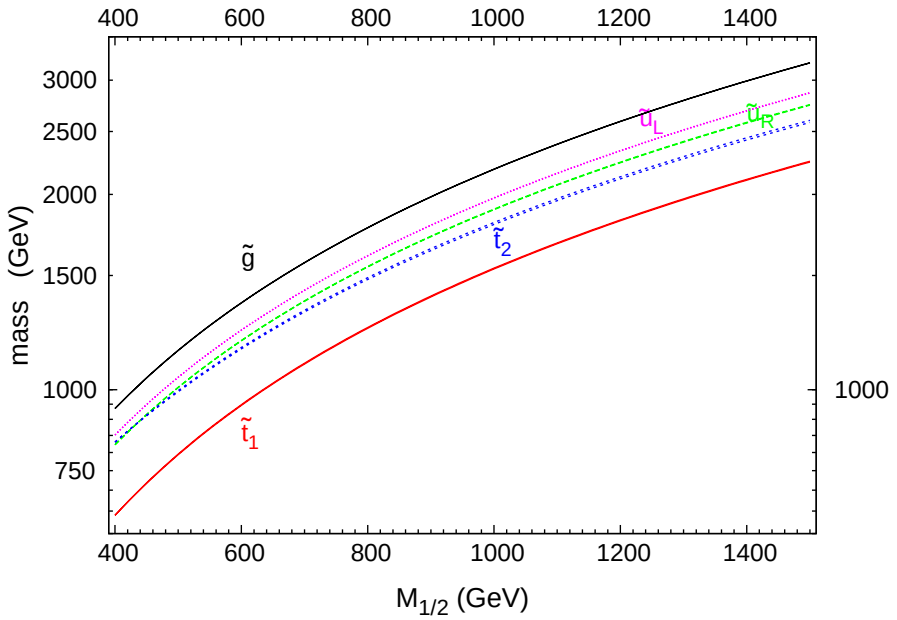

Figure 7: Squark and gluino masses as a function of $M_{1/2}$ within the range obtained by taking $m_0 = 0$ or $m_0 = m_0^{\max}(M_{1/2})$. The states are mass ordered as $m_{\tilde{t}_1} < m_{\tilde{t}_2} < m_{\tilde{u}_R} < m_{\tilde{u}_L} < m_{\tilde{g}}$.

(with $M_2 \approx 0.75 M_{1/2}$). The charginos $\chi_1^\pm$ and $\chi_2^\pm$ are nearly degenerate in mass with, respectively, the wino-like χ_3^0 and the higgsino-like $\chi_{4,5}^0$ states.

For completeness, we have also depicted the masses of the left and right handed selectrons, $\tilde{e}_L$ and $\tilde{e}_R$ (black/full lines), which are degenerate in mass with, respectively, the smuons $\tilde{\mu}_L$ and $\tilde{\mu}_R$. The right-handed states are always lighter than the left-handed ones and the mass pattern is such that $m_{\tilde{e}_L} < m_{\chi_2^0} < m_{\tilde{e}_R}$. Of course, all these states are heavier than the NLSP $\tilde{\tau}_1$ (in fact, $\tilde{e}_L$ is almost degenerate with $\tilde{\tau}_2$). Due to SU(2) symmetry, the sneutrinos have approximately the same masses as the left-handed sleptons.

In Fig. 7, we display the masses of the gluino and of up-type squarks as a function of $M_{1/2}$. Here, the variation of the parameter m_0 in the range $0 \lesssim m_0 \lesssim m_0^{\max}(M_{1/2})$ results only in a hardly visible "width" of the lines. The masses of the c-quarks are degenerate with those of the u-squarks and have not been displayed in the figure.

We first note that the gluino is always heavier than the squarks, a consequence of the small ratio $m_0/M_{1/2}$; this feature has important consequences as will be discussed later. The left- and right-handed up-type squarks are almost degenerate (the mass difference being less than 5%), and also nearly degenerate with the first and second generation down-type squarks, which are not shown in Fig. 7. The top squarks are lighter than the u-squarks, the mass of the lighter stop $\tilde{t}_1$ being $\approx 20\%$ smaller. Thus, $\tilde{t}_1$ is the lightest strongly interacting particle. The bottom squarks have masses somewhat below the heavier stop $\tilde{t}_2$.

Actually, since the singlet sector practically decouples, most of the spectrum could also be obtained in the cMSSM, provided the present values of $M_{1/2}$, m_0 and A_0 are used. We have explicitly verified that the obtained spectra of the non-singlet states for the two points of the cNMSSM parameters discussed in the next subsection agree with those obtained in

the MSSM with the program Suspect [33] (up to small differences due to the treatment of the higher order radiative corrections).

3.4 Examples of spectra

The most relevant features of the sparticle and Higgs spectrum can be represented by two points P1 and P2, for which the distinct cNMSSM inputs, as well as the spectra, are summarized in the left part of Table 1. These two points illustrate the low and intermediate $M_{1/2}$ regime in the cNMSSM.

In the right part of Table 1, we display the resulting spectrum for the Higgs, LSP and NLSP states for $m_0 \neq 0$. While the input $M_{1/2}$ is the same, the input values of A_0 and $\tan\beta$ have been slightly adjusted in order to obtain acceptable values for the dark matter density and the unification of the singlet mass. In the points P1 and P1', the CP-even h_1^0 state is singlet-like, with a somewhat lower value of $m_{h_1^0}$ for P1'. The h_1^0 state is SM-like for P2, while h_1^0 and h_2^0 have a very similar non-singlet components in P2' implying similar couplings to gauge bosons and quarks.

4 Prospects for collider searches

4.1 Sparticle and Higgs decays

The most interesting aspects of the spectrum of the cNMSSM – as compared to the cMSSM – are the presence of a singlino-like LSP with a mass just below the one of the stau NLSP, and the fact that all squarks are lighter than the gluino. The singlino-like LSP with its small coupling to all other sparticles will strongly modify the sparticle decay chains, since now all sparticles will decay via the stau NLSP. Also, squark and gluino decay chains will differ from most MSSM-like scenarios. These two features will have important consequences for sparticle searches at the LHC.

4.1.1 Sparticle decay branching ratios

The branching ratios for the gluinos, squarks, sleptons and charginos/neutralinos are shown in Table 2 for the points P1 and P2 with $m_0 = 0$ (the situation being similar in the primed points with $m_0 \neq 0$). They have been obtained by applying the program SUSYhit [34], which calculates the decay widths and the branching ratios of the Higgs and SUSY particles of the MSSM, to the NMSSM with a practically decoupled singlet sector. A few comments are in order.

– As the gluino $\tilde{g}$ is heavier than all squarks, it can decay via two–body decays into all quark-squark pairs. The branching ratio into $t\,\tilde{t}_1$ final states is somewhat larger ($\sim 20\%$) as a consequence of the larger phase space due to the lighter $\tilde{t}_1$ states.

– All squarks (including the stops) decay into neutralinos or charginos plus the corresponding quark. For right-handed squarks $\tilde{q}_R$ of the first two generations, the branching ratio of the decay $\tilde{q}_R \to \chi_2^0\, q$ is nearly 100%, the χ_2^0 state being dominantly bino-like. In

	P1	P2
$M_{1/2}$ (GeV)	500	1000
m_0 (GeV)	0	0
A_0 (GeV)	-122	-263
$\tan\beta$	26.7	32.2
$\mu_{\rm eff}$ (GeV)	640	1185
M_2 (GeV)	390	790
$m_{h_1^0}$ (GeV)	86	119
$m_{h_2^0}$ (GeV)	116	187
$m_{h_3^0}$ (GeV)	610	1073
$m_{a_1^0}$ (GeV)	149	323
$m_{\chi_1^0}$ (GeV)	122	264
$m_{\chi_2^0}$ (GeV)	206	427
$m_{\chi_3^0}$ (GeV)	388	802
$m_{\chi_{4,5}^0}$ (GeV)	645	1190
$m_{\chi_1^\pm}$ (GeV)	388	801
$m_{\chi_2^\pm}$ (GeV)	658	1198
$m_{\tilde{g}}$ (GeV)	1150	2187
$m_{\tilde{u}_L}$ (GeV)	1044	1973
$m_{\tilde{u}_R}$ (GeV)	1007	1895
$m_{\tilde{t}_1}$ (GeV)	795	1539
$m_{\tilde{t}_2}$ (GeV)	997	1810
$m_{\tilde{b}_1}$ (GeV)	931	1760
$m_{\tilde{b}_2}$ (GeV)	983	1817
$m_{\tilde{e}_L}$ (GeV)	334	654
$m_{\tilde{e}_R}$ (GeV)	190	370
$m_{\tilde{\nu}_l}$ (GeV)	325	650
$m_{\tilde{\tau}_1}$ (GeV)	127	269
$m_{\tilde{\tau}_2}$ (GeV)	343	647
$m_{\tilde{\nu}_\tau}$ (GeV)	318	631

	P1′	P2′
$M_{1/2}$ (GeV)	500	1000
m_0 (GeV)	40	107
A_0 (GeV)	-137	-327
$\tan\beta$	30.2	38.4
$\mu_{\rm eff}$ (GeV)	642	1192
M_2 (GeV)	390	791
$m_{h_1^0}$ (GeV)	64	116
$m_{h_2^0}$ (GeV)	116	127
$m_{h_3^0}$ (GeV)	588	989
$m_{a_1^0}$ (GeV)	149	333
$m_{\chi_1^0}$ (GeV)	107	226
$m_{\tilde{\tau}_1}$ (GeV)	112	235

Table 1: Input parameters and low-energy spectra for four points of the cNMSSM with two distinct $M_{1/2}$ regimes. On the left are Points P1 and P2 with $m_0 = 0$, $M_{1/2} = 500$ GeV and 1 TeV. On the right P1′ and P2′ with $m_0 \neq 0$, for which we only display those masses whose values vary with m_0. In all cases, we have set $\lambda = 0.002$.

the case of the left-handed $\tilde{q}_L$ states, the branching ratios are $\sim \frac{1}{3}$ and $\sim \frac{2}{3}$ for the decays into the neutral $\tilde{q}_L \to q\chi_3^0$ and charged $\tilde{q}_L \to q'\chi_1^-$ wino states, respectively.

– Regarding the decays of the electroweak gauginos, the preferred decay channel of the state χ_2^0 is $\chi_2^0 \to \tilde{\tau}_1\,\tau$ which has a branching ratio of $\sim 90\%$ (for P1) as a result of the more favorable phase space; the remaining $\sim 10\%$ are the decays $\chi_2^0 \to \tilde{l}_R\,l$, where $l = e^\pm$ or $\mu^\pm$. The wino-like χ_3^0 and $\chi_1^\pm$ decay $\sim 50\%$ into first/second generation slepton+lepton states and $\sim 50\%$ into third generation $\tilde{\tau}\tau, \tilde{\nu}_\tau\nu_\tau$ states; the reason for the breaking of lepton

BR (%)	P1	P2
$\tilde{g} \to \tilde{q}_L\, \bar{q}$	17.7	14.4
$\tilde{g} \to \tilde{q}_R\, \bar{q}$	33.6	27.5
$\tilde{g} \to \tilde{b}_1\, \bar{b}$	16.5	12.8
$\tilde{g} \to \tilde{b}_2\, \bar{b}$	10.9	10.3
$\tilde{g} \to \tilde{t}_1\, \bar{t}$	21.2	22.4
$\tilde{g} \to \tilde{t}_2\, \bar{t}$	–	12.5
$\tilde{q}_L \to \chi_3^0\, q$	31.7	32.3
$\tilde{q}_L \to \chi_1^\pm\, q'$	62.7	64.3
$\tilde{q}_R \to \chi_2^0\, q$	99.7	99.9
$\tilde{l}_L \to \chi_2^0\, l$	100	100
$\tilde{l}_R \to l\, \tilde{\tau}_1\, \tau$	$\gtrsim 99$	$\gtrsim 99$
$\tilde{\nu}_l \to \chi_2^0\, \nu_l$	100	100
$\tilde{\nu}_\tau \to \chi_2^0\, \nu_\tau$	13.8	6.8
$\tilde{\nu}_\tau \to \tilde{\tau}_1\, W$	86.2	93.2

BR (%)	P1	P2
$\chi_2^0 \to \tilde{\tau}_1\, \tau$	88.3	74.3
$\chi_2^0 \to \tilde{l}_R\, l$	11.7	25.7
$\chi_3^0 \to \tilde{l}_L\, l$	22.1	28.4
$\chi_3^0 \to \tilde{\nu}_l\, \nu_l$	27.1	29.2
$\chi_3^0 \to \tilde{\tau}_1\, \tau$	24.9	8.8
$\chi_3^0 \to \tilde{\tau}_2\, \tau$	6.9	14.8
$\chi_3^0 \to \tilde{\nu}_\tau\, \nu_\tau$	16.9	18.3
$\chi_1^\pm \to \tilde{\nu}_l\, l$	29.3	29.9
$\chi_1^\pm \to \tilde{l}\, \nu_l$	20.8	27.8
$\chi_1^\pm \to \tilde{\nu}_\tau\, \tau$	18.4	18.9
$\chi_1^\pm \to \tilde{\tau}_1\, \nu_\tau$	24	8.7
$\chi_1^\pm \to \tilde{\tau}_2\, \nu_\tau$	–	14.3

Table 2: Dominant decay modes of the squark, slepton, gluino, neutralino and chargino states for the two points P1 and P2, for which the spectrum is given in Table 1 (and where $\lambda = 0.002$). They have been obtained using SUSYhit [34]; q and l denote first and second generation quarks and leptons, respectively.

universality is again the more favorable phase space.

– Finally, while the left–handed first/second generation sleptons $\tilde{l}_L$ decay to 100% into $l\chi_2^0$ final states, the right-handed sleptons $\tilde{l}_R$ essentially decay via the three–body channel $\tilde{l}_R \to l\, \tilde{\tau}_1\, \tau$; this decay mode has also been discussed in Ref. [35], albeit in a different context. The branching ratio for the two-body decay mode $\tilde{l}_R \to \chi_1^0\, l$ is well below the percent level; the decay into the bino χ_2^0 and a lepton is forbidden by phase space. The reason for the dominance of the three-body decay is that the two–body decay can occur only via the bino-component of $\mathcal{O}(\lambda)$ of the mostly singlino-like χ_1^0, and hence is extremely small, even for the maximally possible values of $\lambda \sim 0.01$ shown in Fig. 3. On the other hand, the three–body decay occurs through the virtual exchange of the bino-like χ_2^0, whose virtuality is not very large as the $\tilde{l}_R$ and χ_2^0 masses are comparable.

Hence, practically *all* sparticle decay chains contain the $\tilde{\tau}_1$ NLSP. The $\tilde{\tau}_1$ life time can be very large, but it will finally decay into the singlino-like LSP and a tau lepton, $\tilde{\tau}_1 \to \chi_1^0\, \tau$.

4.1.2 Displaced vertices

For very small λ, the couplings between the $\tilde{\tau}_1, \chi_1^0$ and τ states might be sufficiently small, resulting into a stau track of $\mathcal{O}(\text{few mm})$ that might be visible [36, 37]. Hence, displaced vertices at high-energy colliders such as the LHC from long-lived staus could be a "smoking gun" signature of the cNMSSM. Here we present some details of the computation and the resulting possible track lengths.

Following Ref. [38], the partial width of the stau decay into the lightest neutralino and tau lepton can be written as

$$\Gamma(\tilde{\tau}_1 \to \chi_1^0 \tau) \;=\; \frac{\rho^{1/2}(m^2_{\tilde{\tau}_1}, m^2_{\tau}, m^2_{\chi_1^0})}{16\pi m^3_{\tilde{\tau}_1}} \left[(a_{11}^2 + b_{11}^2)\, (m^2_{\tilde{\tau}_1} - m^2_{\tau} - m^2_{\chi_1^0}) - 4 a_{11} b_{11} m_{\tau} m_{\chi_1^0} \right], \quad (4.25)$$

where ρ is the phase-space function, $\rho(x,y,z) = x^2 + y^2 + z^2 - 2xy - 2xz - 2yz$, and a_{11}, b_{11} are the $\chi_1^0\, \tilde{\tau}_1\, \tau_{R,L}$ couplings, defined as

$$\begin{aligned} a_{11} \;&=\; -\, g_2 \sqrt{2}\, \tan\theta_{\rm W}\, N_{11}\, \sin\theta_{\tau} - h_{\tau}\, N_{13}\, \cos\theta_{\tau}\,, \\ b_{11} \;&=\; \frac{g_2}{\sqrt{2}}\, (N_{12} + \tan\theta_{\rm W}\, N_{11})\, \cos\theta_{\tau} \; - h_{\tau}\, N_{13}\, \sin\theta_{\tau}\,. \end{aligned} \quad (4.26)$$

h_τ and θ_τ denote the tau Yukawa coupling and stau mixing angle, g_2 the SU(2) coupling constant and N_{1i} denote the composition of the lightest neutralino, $\tilde{\chi}_1^0 = N_{11}\tilde{B} + N_{12}\tilde{W} + N_{13}\tilde{H}_d^0 + N_{14}\tilde{H}_u^0 + N_{15}\tilde{S}$. In the regime of small λ, the bino (N_{11}), wino (N_{12}) and higgsino (N_{13} and N_{14}) components of the mostly singlino-like neutralino χ_1^0 are all proportional to λ [36]. Hence it is convenient to introduce nearly λ-independent coefficients α and β defined as $a_{11}^2 + b_{11}^2 = \lambda^2\, \alpha$ and $2 a_{11} b_{11} = \lambda^2\, \beta$.

In the relevant limits $\Delta m \equiv m_{\tilde{\tau}_1} - m_{\chi_1^0} \ll m_{\tilde{\tau}_1} \sim m_{\chi_1^0}$ and $m_\tau \ll m_{\tilde{\tau}_1} \sim m_{\chi_1^0}$, the expression eq. (4.25) for the stau decay width can be simplified as [36]

$$\Gamma(\tilde{\tau}_1 \to \chi_1^0 \tau) \;\approx\; \lambda^2\, \frac{\sqrt{\Delta m^2 - m_{\tau}^2}}{4\pi m_{\tilde{\tau}_1}}\, (\alpha \Delta m - \beta m_{\tau})\,, \quad (4.27)$$

which summarizes the essential dependence of the stau decay width on λ and Δm.

The coefficients α and β still depend somewhat on $M_{1/2}$ and m_0, and their numerical values smoothly decrease with $M_{1/2}$; for 400 GeV $\lesssim M_{1/2} \lesssim$ 1500 GeV, one has $0.01 \gtrsim \alpha \sim \beta \gtrsim\ 0.0001$. The mass splitting Δm does not only depend on $M_{1/2}$ and m_0: the allowed $2\,\sigma$ range for the relic density in eq. (2.16) allows Δm to vary within a small window at fixed $M_{1/2}$ and m_0, but slightly fluctuating A_0. In the left panel of Fig. 8, we show the corresponding ranges for Δm. Note that for $\Delta m < m_\tau$ the decay of the $\tilde{\tau}_1$ has to proceed via a virtual τ, implying a tiny partial width.

On the right panel of Fig. 8 we plot the reduced stau length of flight, $l^{\rm red}_{\tilde{\tau}_1} = \hbar\, c/\Gamma(\tilde{\tau}_1 \to \chi_1^0 \tau)$, as a function of $M_{1/2}$ for $\lambda = 10^{-3}$. For other values of λ, the reduced length of flight can be obtained by rescaling $l^{\rm red}_{\tilde{\tau}_1}$ by a factor $(10^{-3}/\lambda)^2$. For $M_{1/2} \gtrsim 1200$ GeV and $m_0 = 0$, the lifetime of the stau can be extremely large as a consequence of the NLSP-LSP mass difference approaching the m_τ threshold, which corresponds to the vertical dotted line that extrapolates the upper-most curve in the right panel of Fig. 8.

The stau length of flight in the laboratory frame is given by

$$l_{\tilde{\tau}_1} \;=\; l^{\rm red}_{\tilde{\tau}_1} \sqrt{\beta^2_{\tilde{\tau}_1}/(1 - \beta^2_{\tilde{\tau}_1})}\,, \quad (4.28)$$

where $\beta_{\tilde{\tau}_1} = v_{\tilde{\tau}_1}/c$ is the $\tilde{\tau}_1$ velocity. A realistic estimate of $l_{\tilde{\tau}_1}$ requires the knowledge of $\beta_{\tilde{\tau}_1}$ and hence of the production processes of the lightest stau.

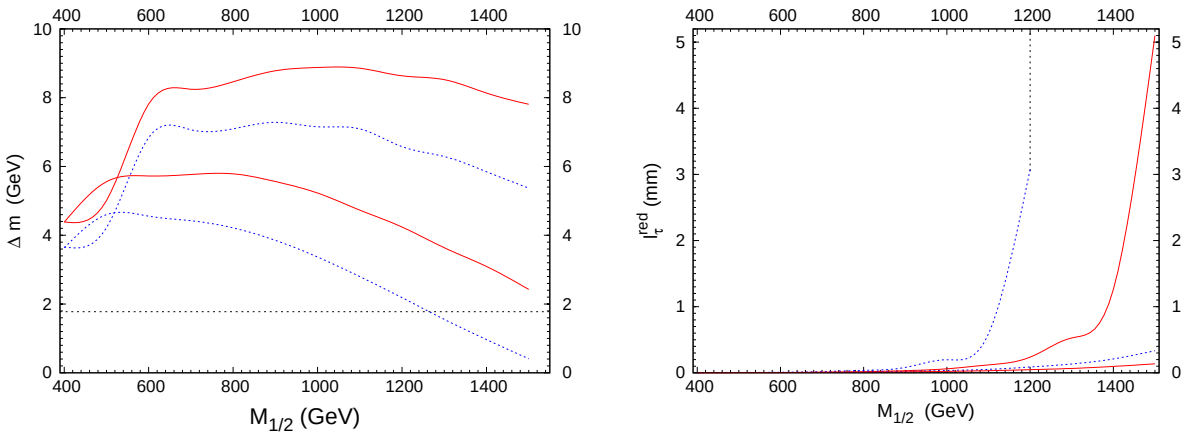

Figure 8: On the left panel, the range of neutralino-stau mass differences Δm which are allowed by the $2\,\sigma$ error bars of the WMAP constraint, as a function of $M_{1/2}$. The lower lines correspond to $m_0 = 0$, the upper ones to its maximal possible value. In each pair, full (red) lines denote the maximal Δm – associated $\Omega_{\chi_1^0} h^2|_{\rm max}$, while dotted (blue) correspond to $\Omega_{\chi_1^0} h^2|_{\rm min}$. The horizontal line denotes m_τ. On the right panel, the maximal and minimal "reduced" stau lengths of flight, $l^{\rm red}_{\tilde\tau_1}$ (in mm), as a function of $M_{1/2}$, for $\lambda = 10^{-3}$, for the neutralino-stau mass differences given in the left panel.

A hint on realistic values for $\beta_{\tilde\tau_1}$ can be obtained from the gauge-mediated SUSY breaking ATLAS benchmark point GMSB5, where it is advocated that over 99% of the staus (which will decay into a gravitino LSP) have $\beta_{\tilde\tau_1} \gtrsim 0.7$ [39].

In Fig. 9, we display the decay length $l_{\tilde\tau_1}$ as a function of $M_{1/2}$ for the choice $m_0 = 0$, taking an intermediate value of Δm within the range presented on the left panel of Fig. 8. We consider two values of $\beta_{\tilde\tau_1}$, and two distinct regimes for λ. As mentioned above, even for λ close to its upper limit (left panel of Fig. 9), visible lengths of flight $l_{\tilde\tau_1}$, of $\mathcal{O}$(mm), are possible for the lightest cNMSSM stau for large $M_{1/2} \sim 1.4$ TeV.

On the right panel of Fig. 9 we consider a smaller value $\lambda \sim 10^{-4}$, and focus on the possibilities within the range of $M_{1/2} < 1$ TeV favored by the data on $(g-2)_\mu$, where one can still obtain a stau length of flight as large as a few centimeters. For larger values of $M_{1/2}$ and $\lambda \lesssim 10^{-4}$, $l_{\tilde\tau_1}$ can become as large as $\mathcal{O}(10\,{\rm cm})$ and even $\mathcal{O}(1\,{\rm m})$.

Long-lived stau NLSPs are also possible in MSSM-like models, if the gravitino is the true LSP. However, at least if $m_{3/2}$ is not much smaller than $M_{\rm SUSY}$, the stau length of flight will always exceed the size of the detector (see [40] for recent analyses of collider signatures of such scenarios). For gauge-mediated SUSY breaking models, where $m_{3/2} \ll M_{\rm SUSY}$, implications of long-lived stau NLSPs for SUSY searches at high energy colliders such as the LHC have been discussed for example Ref. [39]. For the NMSSM, no such studies exist at present.

In any case, although visibly displaced vertices from long-lived stau decays are not an unavoidable prediction within the cNMSSM, they are a very interesting possibility of the parameter space associated to small λ and/or Δm.

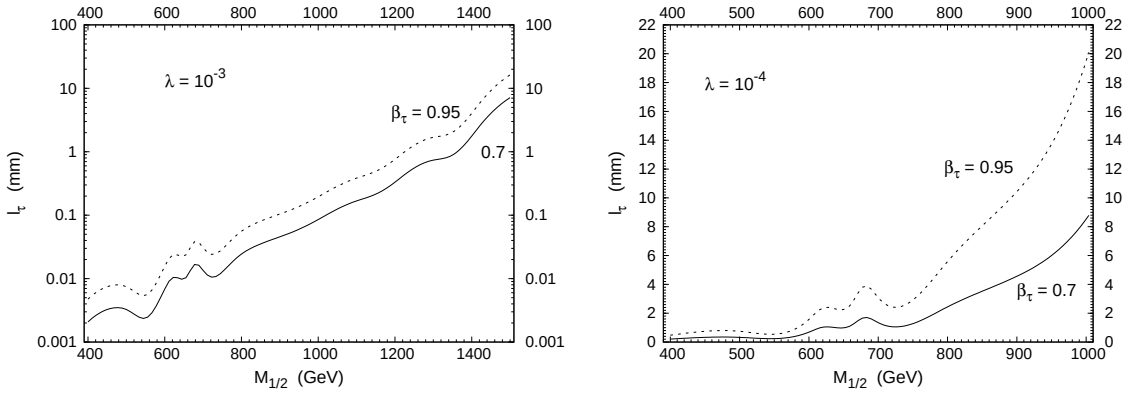

Figure 9: The stau length of flight $l_{\tilde{\tau}_1}$ (in mm), as a function of $M_{1/2}$ (in GeV), for $m_0 = 0$ and $\lambda = 10^{-3}$ (left panel) and $\lambda = 10^{-4}$ (right panel). In both panels, the upper line corresponds to $\beta_{\tilde{\tau}_1} = 0.95$, while for the lower one we have chosen $\beta_{\tilde{\tau}_1} = 0.7$. Note the different scales of the $M_{1/2}$-axis.

4.1.3 Higgs decays

In the cNMSSM, the decay pattern of the non singlet Higgs particles will follow that of the MSSM in the decoupling regime [28].

The lightest non-singlet like CP-even Higgs boson is SM-like with a mass between 115 and 120 GeV, implying that it will dominantly decay into $b\bar{b}$ pairs with a branching ratio larger than $\approx 70\%$, followed by decays into $c\bar{c}, \tau^+\tau^-$ and gg pairs, with branching ratios of the order of 5%. The branching ratio for the decay into a pair of W bosons (one of them being virtual) is less than 10%. The branching ratio for the interesting decay into two photons will be at the level of $\mathrm{BR}(h^{\mathrm{SM}} \to \gamma\,\gamma) \approx 2 \times 10^{-3}$.

The heavier non-singlet Higgs particles h_3^0, a_2^0 (and $h^\pm$) will mainly decay into $b\bar{b}$ and $\tau^+\tau^-$ (tb and $\tau\nu$) pairs. The branching ratios will be 90% and 10% for the hadronic and leptonic decay modes, respectively. Due to the strong enhancement of the b and τ Higgs couplings as a result of the large value of $\tan\beta \gtrsim 30$, the Higgs decays into SUSY particles, as phase space allowed decays into pairs of the lighter neutralinos and sleptons, will be strongly suppressed.

The decays of the singlet-like neutral Higgs bosons (which are unlikely to be produced as will be discussed later) are induced through their (typically small) non-singlet components, implying branching fractions corresponding to a SM-like Higgs.

Higgs-to-Higgs decays, which are a very peculiar possibility within the unconstrained NMSSM and which have been discussed in great detail in Ref. [5], are generally absent in most of the parameter space of the cNMSSM; only for the largest possible values of λ, the lightest CP-even singlet-like Higgs mass can be sufficiently small and its coupling to h_2^0 still sufficiently large as to give rise to a non-negligible $\mathrm{BR}(h_2^0 \to h_1^0\,h_1^0)$. An illustrative example is given by the following choice of input parameters

$$M_{1/2} = 500\,\mathrm{GeV},\ m_0 = 46.5\,\mathrm{GeV},\ A_0 = -142.65\,\mathrm{GeV},\ \tan\beta = 31.72,\ \lambda = 0.0097\,, \tag{4.29}$$

where one obtains $m_{h_1^0} \simeq 50$ GeV and $m_{h_2^0} \simeq 118$ GeV. The dominant h_2^0 branching fractions are then

$$\mathrm{BR}(h_2^0 \to b\,\bar{b}) \,=\, 64.1\%\,, \quad \mathrm{BR}(h_2^0 \to h_1^0\,h_1^0) \,=\, 12.1\%\,. \tag{4.30}$$

The state h_1^0 will mostly decay into $b\bar{b}$ (90%) and $\tau^+\tau^-$ (10%) final states.

4.2 Sparticle and Higgs production at the LHC

Regarding sparticle production at the LHC, we summarize in Table 3 the cross sections for the most relevant production channels for the points P1 and P2 defined in Table 1. These have been obtained by using the Fortran code Prospino [41], which calculates the cross sections for sparticle production at hadron colliders to next-to-leading order in perturbation theory, for the non-singlet sector of the cNMSSM.

The largest cross sections are expected for the strongly interacting production processes $pp \to \tilde{q}\tilde{g}$, $\tilde{q}\tilde{q}$ and $\tilde{q}\tilde{q}^*$, where $\tilde{q}$ denotes all squarks but the stop. One obtains $\sigma_{\tilde{q}\tilde{g}} \simeq 0.67$ pb, $\sigma_{\tilde{q}\tilde{q}} \simeq 0.44$ pb and $\sigma_{\tilde{q}\tilde{q}^*} \simeq 0.22$ pb for the points P1 (and P1') with $M_{1/2} = 500$ GeV, while for the point P2 (likewise for P2') with $M_{1/2} = 1000$ GeV, only $\sigma_{\tilde{q}\tilde{q}} \simeq 0.01$ pb, $\sigma_{\tilde{q}\tilde{g}} = 0.004$ pb and $\sigma_{\tilde{q}\tilde{q}^*} = 0.002$ pb are expected. Assuming the LHC high luminosity option of $\mathcal{L} = 100$ fb^{-1}, one obtains 10^4 to 10^5 events for scenario P1, but only 10^2 to 10^3 events for scenario P2 (before efficiency cuts are applied). The yield for gluino pair production, $q\bar{q}/gg \to \tilde{g}\tilde{g}$, is much smaller as a result of the larger gluino mass.

As discussed in Section 4.1, all gluinos will decay into squarks. Squarks decay into quarks and the wino-like neutralinos or charginos, which then cascade mostly into the lighter $\tilde{\tau}$ NLSP. Hence all sparticle decay chains contain the $\tilde{\tau}_1$ NLSP, which will finally decay into the singlino-like LSP, $\tilde{\tau}_1 \to \chi_1^0\,\tau$, possibly leading to a displaced vertex.

The simplest possible squark decay cascades at the LHC – originating mostly from right-handed squarks of the first generation $\tilde{q}_R$ – are thus of the form

$$\tilde{q}_R \;\to\; q\,\chi_2^0 \;\begin{array}{l}\nearrow \\ \searrow\end{array}\; \begin{array}{lll} q\tilde{\tau}_1\tau & \to\; q\tau\tau\chi_1^0 & (\mathrm{P1}:88\%;\ \mathrm{P2}:74\%) \\ q\tilde{l}_R l \to q l\tilde{\tau}_1\tau & \to\; q\tau\tau\chi_1^0 + \ell & (\mathrm{P1}:12\%;\ \mathrm{P2}:25\%) \end{array} \tag{4.31}$$

where, according to Table 2, the first case occurs $\sim 88\%$ for point P1 and $\sim 74\%$ for point P2. The second case occurs only $\sim 12\%$ and $\sim 25\%$ for P1 and P2, respectively. These cascades typically lead to events with 3 jets per $\tilde{q}_R$ (one hard quark and two tau jets, also potentially hard, depending on the momentum of the decaying χ_2^0 neutralino), but the leptonic decays of the τ can possibly also be used.

As can be seen from eq. (4.31), right-handed squark cascade decays containing a lepton in the final state are clearly sub-dominant. In the case of left-handed squarks, the decays would lead to more e, μ lepton final states, since $\tilde{q}_L$ mainly decays into $q\chi_3^0$ and $q\chi_1^\pm$. The wino-like neutralino χ_3^0 and chargino $\chi_1^\pm$ decay either directly to $\tilde{\tau}_1$ and $\tilde{\nu}_\tau$ (the latter decaying predominantly into $\tilde{\tau}_1 W$) or to $\tilde{l}_L, \tilde{\nu}_l$. These then decay into $l\chi_2^0$ and $\nu\chi_2^0$, respectively. The bino-like χ_2^0 would dominantly lead to $\tilde{\tau}_1\tau$ and, to a minor extent, to $\tilde{l}_R l \to ll\tilde{\tau}_1\tau$ final states. Therefore, one has a non-negligible probability for one, two, three and even four e, μ leptons in the final states. For instance, the branching ratios into the four lepton topology would be $\approx 1\%$ and $\approx 2\%$ for, respectively, points P1 and P2.

σ (pb)	P1	P2
$\tilde{g}\,\tilde{g}$	9.5×10^{-2}	2.14×10^{-4}
$\tilde{g}\,\tilde{q}$	0.668	4.28×10^{-3}
$\tilde{q}\,\tilde{q}$	0.436	9.21×10^{-3}
$\tilde{q}\,\tilde{q}^*$	0.221	1.64×10^{-3}
$\tilde{t}_1\,\tilde{t}_1^*$	3.69×10^{-2}	2.63×10^{-4}
$\tilde{l}_L\,\tilde{l}_L^*$	3.4×10^{-3}	1.62×10^{-3}
$\tilde{l}_R\,\tilde{l}_R^*$	1.17×10^{-2}	8.87×10^{-4}
$\tilde{\nu}_l\,\tilde{\nu}_l^*$	3.58×10^{-3}	1.53×10^{-4}
$\tilde{\tau}_1\,\tilde{\tau}_1^*$	4.8×10^{-2}	3.46×10^{-3}
$\chi_2^0\,\chi_2^0$	1.1×10^{-3}	6.22×10^{-5}
$\chi_2^0\,\chi_3^0$	1.73×10^{-4}	8.67×10^{-6}
$\chi_2^0\,\chi_1^\pm$	5.37×10^{-4}	6.53×10^{-5}
$\chi_3^0\,\chi_3^0$	1.79×10^{-3}	5.74×10^{-5}
$\chi_3^0\,\chi_1^\pm$	6.51×10^{-2}	7.49×10^{-3}
$\chi_1^+\,\chi_1^-$	3.53×10^{-2}	1.17×10^{-3}

Table 3: Production cross sections (in pb) for strongly (upper part) and weakly (lower part) interacting sparticles at the LHC in the points P1 and P2 defined in Table 1, as obtained with the program Prospino [41]. Here $\tilde{q}$ denotes all squarks but the stop, and $l = \mu$ or e.

For chargino and neutralino or mixed pair production, the cross sections are also shown in the lower part of Table 3; they are sizable enough only for point P1, where the phase space is not too penalizing. In the case of $\chi_1^\pm\chi_1^\mp$ and $\chi_3^0\chi_1^\pm$, they lead to a few thousand events for an integrated luminosity of $\mathcal{L} = 100$ fb^{-1}, before cuts are applied. However, since charginos and neutralinos also dominantly cascade into $\tilde{\tau}$ lepton final states, only a very small fraction leads to the nice signature of multi e, μ lepton events.

The cross sections for the Drell-Yan production of slepton pairs is of the same order as the one of charginos and neutralinos, the highest one being $p\bar{p} \to \tilde{\tau}_1\tilde{\tau}_1^*$ pair production (with $\sigma \approx 50$ fb for P1, where $m_{\tilde{\tau}_1} \approx 130$ GeV) as a result of the more favorable phase space[2].

Since cascade decays leading to e, μ lepton final states will be generally rare in the cNMSSM, the measurements of the sparticle masses from kinematical endpoints and, thus, the determination of some of the soft–SUSY breaking parameters, cannot be performed

[2]In fact, at the Tevatron, the only process which might have a significant production cross section is the pair production of the lighter stau: one would have $\sigma(p\bar{p} \to \tilde{\tau}_1\tilde{\tau}_1^*) \approx 15$ fb for $m_{\tilde{\tau}_1} \approx 100$ GeV. The final state would then essentially consist of missing energy and two tau final states, the latter potentially decaying into muons with large impact parameters, since the $\tilde{\tau}_1$ lifetime can be e.g. of the order of 20 ps for $m_{\tilde{\tau}_1} \approx 100$ GeV and $\lambda \approx 10^{-5}$. Such events would share some (but definitely not all) of the peculiarities of the displaced multi-muon events recently reported by (part of) the CDF collaboration [42]. However, in our case only a handful of events would have been produced and the τ multiplicity would be far too small.

with the same level of accuracy as it would be the case for the MSSM. Note also that, in most cases, one of the leptons originates from the three-body $\tilde{l}_R \to l\tilde{\tau}_1\tau$ decay.

Hence, a SUSY signal can certainly be observed at the LHC by looking, for instance, for final states with hard jets plus a large amount of missing energy. However, precision measurements through the endpoints of decay spectra will be more complicated to perform in the case of τ final states which are overwhelming in the cNMSSM.

Finally, let us make a few comments on Higgs detection in this scenario. As previously discussed, in most cases the cNMSSM Higgs sector reduces to the one of the MSSM in the decoupling regime. The SM-like CP-even Higgs boson with its mass in the 115–120 GeV range can be discovered first at the Tevatron (if enough integrated luminosity is collected) in the Higgs–strahlung process $pp \to W$+Higgs leading to $l\nu b\bar{b}$ final states. At the LHC, the most relevant production and decay processes will be the gluon-gluon and vector boson fusion, $gg \to$ Higgs and $qq \to qq$+Higgs, with the Higgs boson decaying into two photons (and possibly $\tau^+\tau^-$ final states in the vector boson fusion process).

We recall the phenomenon of the "cross-over" for certain values of $M_{1/2}$ and m_0, which corresponds to two nearly degenerate CP-even Higgs bosons sharing their couplings to the SM gauge bosons, quarks and leptons. This is the case illustrated by the last point P2' of Table 1, where the lightest Higgs bosons h_1^0 and h_2^0 have very similar singlet/doublet components ~ 0.7, i.e. similar production cross sections and branching fractions, and a mass splitting of about 10 GeV. In principle, both states could be observed[3]. For smaller values of λ, the mass splitting in the cross-over region can be considerably smaller, less than 1 GeV for $\lambda \lesssim 10^{-4}$. Then, the sum of both Higgs bosons gives rise to a single SM-like Higgs boson peak, which can be quite difficult to resolve at the LHC.

The heavier non-singlet Higgs particles have significant couplings to SM down-type fermions in view of the large values of $\tan\beta \gtrsim 30$. They can be observed in associated production with $b\bar{b}$ pairs and decays into $\tau^+\tau^-$ pairs for the neutral particles, and associated production with tb pairs with decays into $\tau\nu$ in the case of charged Higgs bosons. However, this is only possible for low values of $M_{1/2} \lesssim 700$ GeV, which lead to light enough Higgs particles with sufficient production cross sections. In any case, a very high luminosity is required to observe these particles.

Apart from the "cross-over" region, the singlet-like Higgs states are generally inaccessible as they couple too weakly to SM fermions and gauge bosons. Only if the mass of a singlet-like CP-even Higgs boson h_1^0 is sufficiently small and λ sufficiently large, as is the case for the point given in eq. (4.29), the branching ratio $h_2^0 \to h_1^0 h_1^0$ of the then SM-like h_2^0 can be sizable (leading to a slightly reduced $h_2^0 \to \gamma\gamma$ branching ratio). Whether this production of h_1^0 leading to difficult $4b, 2\tau 2b$ and 4τ final state topologies could be detected [5], needs also a dedicated detailed investigation.

[3]The situation here is similar to the MSSM intense coupling regime discussed in Ref. [43] in which all neutral MSSM bosons are close in mass; however, in the cNMSSM, the couplings of the lighter CP-even states to down-type fermions are not particularly enhanced.

4.3 Searches at the ILC

Due to the relatively heavy Higgs and sparticle spectrum, a multi–TeV e^+e^- collider would be required to produce all the states of the constrained NMSSM. At a 500 GeV ILC, only the two lighter neutralinos and the right-handed sleptons can be produced even for $M_{1/2} \lesssim 500$ GeV. The production of wino-like charginos and neutralinos as well as the left-handed sleptons would need a larger center of mass (c.m.) energy of ≈ 1 TeV. The detection of the various SUSY states would be straightforward in the clean environment of the ILC. In particular, a $\tilde{\tau}_1$ nearly degenerate with the LSP can be detected, as shown in detailed simulations for somewhat similar MSSM scenarios [44, 45]. The masses of the SUSY particles could be accurately determined, at least through threshold scans, as has been discussed in detail in Ref. [45], and a clear distinction between the cNMSSM and other scenarios could be made.

As far as the Higgs sector is concerned, only the lighter CP–even and CP–odd Higgs states would be kinematically accessible at an ILC with a c.m. energy less than 1 TeV. The SM-like Higgs particle can be easily detected and its properties probed in detail, the Higgs mass range around ≈ 120 GeV being the ideal one for a 500 GeV ILC [45]. The scenario with sizable singlet/doublet mixing between the h_1^0 and h_2^0 states can be probed in the Higgs-strahlung process, $e^+e^- \to Z$+Higgs, where the separate Higgs states can be disentangled even if they are nearly degenerate in mass, as the resolution on the Higgs masses in this process is smaller than 100 MeV [45]. The scenario of eq. (4.29), in which there is a light CP-even Higgs particle, allows the $h_2^0 \to h_1^0 h_1^0$ decay to occur, which can also be probed in the Higgs-strahlung process $e^+e^- \to h_2^0 Z \to \mu^+\mu^- b\bar{b}b\bar{b}$, and both h_1^0 and h_2^0 masses could be accurately determined. The singlet-like state a_1^0 could be also accessible in the pair production process $e^+e^- \to h_2^0 a_1^0 \to b\bar{b}b\bar{b}$ unless the a_1^0 mass is too large or the coupling λ prohibitively tiny.

4.4 Direct and indirect detection of dark matter

For completeness, let us comment on the prospects for detecting the singlino-like LSP χ_1^0 (with non-singlet components of $\mathcal{O}(\lambda)$) in astroparticle experiments. For the direct LSP detection via χ_1^0-nuclei interactions, the prospects are quite dim: due to the very small values of λ that are required from compatibility of the Higgs sector with LEP bounds, one finds extremely small WIMP-nucleon cross sections[4]. We computed these cross sections using the recent version of the dark matter code MicrOMEGAS [47], adapted to the NMSSM. The result is that the relevant values for the spin-independent and spin-dependent proton and neutron interaction cross-sections are always below $\sim 10^{-13}$ pb, implying an expected number of events smaller than $\mathcal{O}(10^{-8\div-9})$/day/kg for both ^{73}Ge and ^{131}Xe nuclei, and less than $\mathcal{O}(10^{-11\div-12})$/day/kg for ^{3}He.

Furthermore, since χ_1^0 has extremely small couplings to SM fermions and gauge bosons, the annihilation cross sections of χ_1^0 into SM particles are always extremely small. The only significant channel could be the annihilation process $\chi_1^0\chi_1^0 \to a_1^0$ with the CP-odd singlet-

[4]In different studies [18, 46], large direct detection cross sections have been obtained for the case of the non-constrained or semi-constrained NMSSM. The large cross sections were associated to lighter χ_1^0 and larger values of λ, which are not possible in the present case.

like a_1^0 state being sufficiently light to be produced on–shell. However, the $a_1^0\chi_1^0\chi_1^0$ coupling is proportional to κ which is tiny in our case, $\kappa \lesssim 10^{-3}$.

Thus all cross sections involving the singlino LSP are extremely small; in other words, the fully constrained cNMSSM can be excluded by the direct or indirect detection of a WIMP-like dark matter candidate.

5 Summary and conclusions

Due to its simplicity, namely a scale invariant superpotential and universal SUSY-breaking terms at the GUT scale, the cNMSSM is a very attractive supersymmetric extension of the standard model. We have found that for small values of the NMSSM specific Yukawa coupling, $\lambda \lesssim 10^{-2}$, the cNMSSM can satisfy all present phenomenological constraints including LEP constraints on the Higgs sector. The correct dark matter relic density is obtained for small m_0 and A_0 as compared to $M_{1/2}$. Moreover, in the region $M_{1/2} \approx 550 - 600$ GeV, the deviation of $(g-2)_\mu$ from its SM model value and the two excesses of Higgs-like events observed at LEP can be simultaneously explained.

The cNMSSM sparticle spectrum allows to discriminate it from most versions of the MSSM: all squarks are lighter than the gluino, and due to the weakly coupled singlino-like LSP and the stau NLSP, the latter will show up in practically all sparticle decay cascades. In some regions of the parameter space, the stau lifetime can be sufficiently large, possibly leading to visibly displaced vertices.

The mass of the SM-like CP-even Higgs boson is constrained to lie in the 115 – 120 GeV range, and for certain regions in parameter space it could strongly mix with the singlet-like Higgs state. In a small – different – region of the parameter space, decays of the SM-like CP-even Higgs boson into two singlet-like Higgs states are possibly detectable at an ILC.

Note that the model is very predictive: as it becomes clear from Figs. 6 and 7, the measurement of one sparticle mass (or mass difference) would allow to predict quite accurately the complete remaining sparticle spectrum. On the other hand, due to the singlino-like LSP together with small λ, dark matter detection signals can rule out the present model.

Hopefully, the cNMSSM can be tested in the near future at the LHC. To this end the sensitivities of the ATLAS and CMS detectors to sparticle decay cascades involving the stau NLSP should be thoroughly studied.

Acknowledgements

We acknowledge support from the French ANR project PHYS@COL&COS and discussions with S.F. King, S. Moretti and W. Porod. AD is grateful to the Alexander von-Humboldt Foundation (Germany) and to the theory group in Bonn for the hospitality extended to him.

References

[1] P. Fayet, Nucl. Phys. B **90** (1975) 104; Phys. Lett. B **64** (1976) 159; Phys. Lett. B **69** (1977) 489 and Phys. Lett. B **84** (1979) 416; H.P. Nilles, M. Srednicki and D. Wyler,

Phys. Lett. B **120** (1983) 346; J.M. Frere, D.R. Jones and S. Raby, Nucl. Phys. B **222** (1983) 11; J.P. Derendinger and C.A. Savoy, Nucl. Phys. B **237** (1984) 307; J. Ellis, J. Gunion, H. Haber, L. Roszkowski and F. Zwirner, Phys. Rev. D **39** (1989) 844; M. Drees, Int. J. Mod. Phys. A **4** (1989) 3635.

[2] U. Ellwanger, M. Rausch de Traubenberg and C.A. Savoy, Phys. Lett. B **315** (1993) 331 [arXiv:hep-ph/9307322]; Z. Phys. C **67** (1995) 665 [arXiv:hep-ph/9502206] and Nucl. Phys. B **492** (1997) 307 [arXiv:hep-ph/9611251].

[3] T. Elliott, S.F. King and P. White, Phys. Lett. B **351** (1995) 213 [arXiv:hep-ph/9406303]; S.F. King and P. White, Phys. Rev. D **52** (1995) 4183 [arXiv:hep-ph/9505326].

[4] J.E. Kim and H.P. Nilles, Phys. Lett. B **138** (1984) 150.

[5] For a recent discussion and more references, see A. Djouadi *et al.*, JHEP **0807** (2008) 002 [arXiv:0801.4321 [hep-ph]].

[6] A.H. Chamseddine, R. Arnowitt and P. Nath, Phys. Rev. Lett. **49** (1982) 970; R. Barbieri, S. Ferrara and C. Savoy, Phys. Lett. B **119** (1982) 343; L. Hall, J. Lykken and S. Weinberg, Phys. Rev. D **27** (1983) 2359.

[7] C. Hugonie, G. Belanger and A. Pukhov, JCAP **0711** (2007) 009 [arXiv:0707.0628 [hep-ph]].

[8] D. N. Spergel *et al.* [WMAP Collaboration], Astrophys. J. Suppl. **170** (2007) 377 [arXiv:astro-ph/0603452].

[9] U. Ellwanger, J. F. Gunion and C. Hugonie, JHEP **0502** (2005) 066; U. Ellwanger and C. Hugonie, Comput. Phys. Commun. **175** (2006) 290 [arXiv:hep-ph/0508022] and Comput. Phys. Commun. **177** (2007) 399 [arXiv:hep-ph/0612134]; (see also the web site http://www.th.u-psud.fr/NMHDECAY/nmssmtools.html).

[10] G. Belanger, F. Boudjema, C. Hugonie, A. Pukhov and A. Semenov, JCAP **0509** (2005) 001 [arXiv:hep-ph/0505142]; G. Belanger, F. Boudjema, A. Pukhov and A. Semenov, Comput. Phys. Commun. **174** (2006) 577 [arXiv:hep-ph/0405253].

[11] A. Djouadi, U. Ellwanger and A. M. Teixeira, Phys. Rev. Lett. **101** (2008) 101802 [arXiv:0803.0253 [hep-ph]].

[12] S. Schael *et al.* [ALEPH Collaboration and DELPHI Collaboration and L3 Collaboration and OPAL Collaboration], Eur. Phys. J. C **47** (2006) 547 [arXiv:hep-ex/0602042].

[13] A. B. Lahanas and D. V. Nanopoulos, Phys. Rept. **145**, 1 (1987); N. Dragon, U. Ellwanger and M. G. Schmidt, Prog. Part. Nucl. Phys. **18** (1987) 1.

[14] M. A. Luty and R. Sundrum, Phys. Rev. D **65** (2002) 066004 [arXiv:hep-th/0105137]; M. Luty and R. Sundrum, Phys. Rev. D **67** (2003) 045007 [arXiv:hep-th/0111231]; M. Dine, P. J. Fox, E. Gorbatov, Y. Shadmi, Y. Shirman and S. D. Thomas, Phys. Rev.

D **70** (2004) 045023 [arXiv:hep-ph/0405159]; M. Schmaltz and R. Sundrum, JHEP **0611** (2006) 011 [arXiv:hep-th/0608051].

[15] G. Bennett *et al.*, Phys. Rev. D **73** (2006) 072003 [arXiv:hep-ex/0602035]; for a recent review see Z. Zhang, "Muon g-2: a mini review," arXiv:0801.4905 [hep-ph].

[16] R. Barate *et al.* [LEP Working Group for Higgs boson searches and ALEPH Collaboration and DELPHI Collaboration and L3 Collaboration and OPAL Collaboration], Phys. Lett. B **565** (2003) 61 [arXiv:hep-ex/0306033].

[17] B. Allanach *et al.*, "SUSY Les Houches Accord 2," arXiv:0801.0045 [hep-ph].

[18] C. Balazs and D. Carter, "Discovery potential of the next-to-minimal supergravity motivated model," arXiv:0808.0770 [hep-ph].

[19] Particle Data Group [W.-M. Yao *et al.*], J. Phys. G **33** (2006) 1.

[20] U. Ellwanger and C. Hugonie, Phys. Lett. B **457** (1999) 299 [arXiv:hep-ph/9902401].

[21] S. A. Abel and C. A. Savoy, Nucl. Phys. B **532** (1998) 3 [arXiv:hep-ph/9803218].

[22] See for instance, J.R. Ellis, T. Falk, K. Olive and M. Srednicki, Astropart. Phys. **13** (2000) 181 [hep-ph/9905481].

[23] B. Ananthanarayan and P.N. Pandita, Phys. Lett. B **353** (1995) 70 [arXiv:hep-ph/9503323]; Phys. Lett. B **371** (1996) 245 [arXiv:hep-ph/9511415]; Int. J. Mod. Phys. A **12** (1997) 2321 [arXiv:hep-ph/9601372].

[24] K. Griest and D. Seckel, Phys. Rev. D **43** (1991) 3191.

[25] G. Hiller, Phys. Rev. D **70** (2004) 034018 [arXiv:hep-ph/0404220]; F. Domingo and U. Ellwanger, JHEP **0712** (2007) 090 [arXiv:0710.3714 [hep-ph]].

[26] M. Davier, talk given at the Xth International Workshop on tau lepton physics, Novosibirsk, Russia, September 22–25, 2008.

[27] F. Domingo and U. Ellwanger, JHEP **0807** (2008) 079 [arXiv:0806.0733 [hep-ph]].

[28] For a detailed discussion of the SM and MSSM Higgs sectors, see: A. Djouadi, Phys. Rep. **457** (2008) 1 [hep-ph/0503172]; Phys. Rep. **459** (2008) 1 [hep-ph/0503173].

[29] H. Flaecher et al., "Gfitter - Revisiting the Global Electroweak Fit of the Standard Model and Beyond," arXiv:0811.0009 [hep-ph].

[30] M. Drees, Phys. Rev. D **71** (2005) 115006 [arXiv:hep-ph/0502075]; G.L. Kane *et al.*, Phys. Rev. D**71** (2005) 035006 [arXiv:hep-ph/0407001]; S.-G. Kim *et al.*, Phys. Rev. D**74** (2006) 115016 [arXiv:hep-ph/0609076]; A. Belyaev *et al.*, Phys. Rev. Lett. **100** (2008) 061801 [arXiv:hep-ph/0609079].

[31] R. Dermisek and J. F. Gunion, Phys. Rev. D **73** (2006) 111701 [arXiv:hep-ph/0510322].

[32] G. Degrassi *et al.*, Eur. Phys. J. C **28** (2003) 133 [arXiv:hep-ph/0212020]; B. Allanach *et al.*, JHEP **0409** (2004) 044 [arXiv:hep-ph/0406166].

[33] A. Djouadi, J.L. Kneur and G. Moultaka, Comput. Phys. Commun. **176** (2007) 426 [hep-ph/0211331].

[34] A. Djouadi, M. M. Muhlleitner and M. Spira, Acta Phys. Polon. B **38** (2007) 635 [arXiv:hep-ph/0609292].

[35] S. Ambrosanio, G. D. Kribs and S. P. Martin, Nucl. Phys. B **516** (1998) 55 [arXiv:hep-ph/9710217]; S. Kraml and D. T. Nhung, JHEP **0802** (2008) 061 [arXiv:0712.1986 [hep-ph]].

[36] U. Ellwanger and C. Hugonie, Eur. Phys. J. C **5** (1998) 723 [arXiv:hep-ph/9712300].

[37] F. Franke and H. Fraas, Z. Phys. C **72** (1996) 309 [arXiv:hep-ph/9511275]; U. Ellwanger and C. Hugonie, Eur. Phys. J. C **13** (2000) 681 [arXiv:hep-ph/9812427]; V. Barger, P. Langacker and G. Shaughnessy, Phys. Lett. B **644** (2007) 361 [arXiv:hep-ph/0609068] and Phys. Rev. D **75** (2007) 055013 [arXiv:hep-ph/0611239].

[38] A. Bartl, H. Eberl, S. Kraml, W. Majerotto and W. Porod, Z. Phys. C **73** (1997) 469 [arXiv:hep-ph/9603410]; S. Kraml and W. Porod, Phys. Lett. B **626** (2005) 175 [arXiv:hep-ph/0507055].

[39] M. Terwort [ATLAS Collaboration and CMS Collaboration], "Searches for GMSB at the LHC," arXiv:0805.2524 [hep-ex].

[40] A. De Roeck, J. R. Ellis, F. Gianotti, F. Moortgat, K. A. Olive and L. Pape, Eur. Phys. J. C **49** (2007) 1041 [arXiv:hep-ph/0508198]; J. R. Ellis, A. R. Raklev and O. K. Oye, JHEP **0610** (2006) 061 [arXiv:hep-ph/0607261].

[41] W. Beenakker, R. Hopker and M. Spira, "PROSPINO: A program for the PROduction of Supersymmetric Particles In Next-to-leading Order QCD," arXiv:hep-ph/9611232.

[42] T. Aaltonen *et al.* [CDF Collaboration], "Study of multi-muon events produced in p-pbar collisions at sqrt(s)=1.96 TeV," arXiv:0810.5357 [hep-ex]; P. Giromini *et al.*, "Phenomenological interpretation of the multi-muon events reported by the CDF collaboration," arXiv:0810.5730 [hep-ph].

[43] E. Boos *et al.*, Phys. Rev. D **66** (2002) 055004 [arXiv:hep-ph/0205160].; E. Boos, A. Djouadi and A. Nikitenko, Phys. Lett. B **578** (2004) 384 [arXiv:hep-ph/0307079].

[44] H.-U. Martyn, Eur. Phys. J. **C48** (2006) 15 [arXiv:hep-ph/0605257]; P. Bambade, M. Berggren, F. Richard and Z. Zhang, "Experimental implications for a linear collider of the SUSY dark matter scenario," arXiv:hep-ph/0406010; E. Baltz *et al.*, Phys. Rev. D **74** (2006) 103521 [arXiv:hep-ph/0602187].

[45] A. Djouadi, J. Lykken, K. Moening, Y. Okada, M. Oreglia, Y. Yamsashita [conv.] *et al.*, "ILC Reference Design Report" 2: Physics at the ILC, arXiv:0709.1893 [hep-ph].

[46] J. F. Gunion, D. Hooper and B. McElrath, Phys. Rev. D **73** (2006) 015011 [arXiv:hep-ph/0509024]; D. G. Cerdeno, E. Gabrielli, D. E. Lopez-Fogliani, C. Munoz and A. M. Teixeira, JCAP **0706** (2007) 008 [arXiv:hep-ph/0701271]; G. Belanger, C. Hugonie and A. Pukhov, "Precision measurements, dark matter direct detection and LHC Higgs searches in a constrained NMSSM," arXiv:0811.3224 [hep-ph].

[47] G. Belanger, F. Boudjema, A. Pukhov and A. Semenov, "Dark matter direct detection rate in a generic model with micrOMEGAs2.1," arXiv:0803.2360 [hep-ph].